UNIVERSITY OF CALIFORNIA, SAN DIEGO

Automated Micro-Tracking Planar Solar Concentrators

A thesis submitted in partial satisfaction of the
requirements for the degree Master of Science

in

Electrical Engineering (Photonics)

by

Justin Matthew Hallas

Committee in charge:

Professor Joseph E. Ford, Chair
Professor Clark Guest
Professor George Papen

2011

The Thesis of Justin Matthew Hallas is approved and it is acceptable in quality and form for publication on microfilm and electronically:

_____

_____

_____

Chair

University of California, San Diego

2011

DEDICATION

To my wife, Ysabelle, for her unending support and encouragement.

TABLE OF CONTENTS

LIST OF ABBREVIATIONS

λ	Wavelengths of Light (unit)
CPV	Concentrated Photovoltaics
F	Focal Length
F/#	F-number
PMSC	Planar Micro-optic Solar Concentrator
TIR	Total Internal Reflection
µm	microns (unit)
UV	ultra-violet

LIST OF FIGURES

ACKNOWLEDGEMENTS

I would like to acknowledge all of the people who helped me in the creation of this thesis. Thanks go to Professor Joe Ford for providing sage advice and for creating an environment of mutual respect that made my time in graduate school enjoyable, to Eric Tremblay for always answering my questions about ZEMAX and for making a great template from which this thesis is based, to Jason Karp for the many long discussions about this subject matter that, I think, helped to clarify it for us both, and to Katherine Baker for assistance with ZEMAX simulations.

VITA

2008 — Bachelor of Science in Electrical Engineering
University of California, San Diego

2011 — Master of Science in Electrical Engineering (Photonics)
University of California, San Diego

PUBLICATIONS

J. M. Hallas, J. H. Karp, K. A. Baker, E. J. Tremblay, and J. E. Ford, "Micro-tracking of planar micro-optic solar concentrator," Optics Express (in preparation).

K. A. Baker, J. H. Karp, E. J. Tremblay, J. M. Hallas, and J. E. Ford, "Reactive self-tracking solar concentration: design and materials characterization," Energy Express (in preparation).

J. H. Karp, E. J. Tremblay, J. M. Hallas, and J. E. Ford, "Orthogonal and secondary concentration in planar micro-optic solar collectors," Opt. Express 19, A673-A685 (2011)

B. R. Nadler, J. H. Karp, J. M. Hallas and J. E. Ford, "Planar Micro-Optic Tracking Receiver for Free-Space Data Transmission," Journal of Lightwave Technology (in preparation).

J. M. Hallas, J. H. Karp, E. J. Tremblay and J. E. Ford, "Lateral translation micro-tracking of planar micro-optic solar concentrator", Proc. SPIE 7769, 776904 (2010)

NEWS ARTICLES

V. C. Coffey "Solar Concentrators: Using optics to boost photovoltaics," Optics and Photonics News, Vol. 22, Issue 1, pp. 22-27 (2011).

PATENT

J. E. Ford, J. Karp, E. Tremblay, and J. Hallas, "System and method for solar energy capture and related method of manufacturing", patent pending and licensed

ABSTRACT OF THE THESIS

Automated Micro-Tracking Planar Solar Concentrators

by

Justin Matthew Hallas

Master of Science in Electrical Engineering (Photonics)

University of California, San Diego, 2011

Professor Joseph E. Ford, Chair

One aim of solar concentrators is to reduce the cost of a solar power systems by reducing the amount of expensive semiconductor used in exchange for optical concentrating components and tracking mechanics. Solar trackers rotate the solar panel or concentrator so that direct normal incidence is maintained throughout the day. As concentration increases, so does the required complexity and precision of the tracking mechanics. This increased precision results in a larger fraction of the total system cost in tracking. In this thesis I will present an alternative to large-scale two-axis mechanical trackers that relies on the unique geometry of the planar micro-optic solar concentrator.

The planar micro-optic solar concentrator [1] consists of a lens array mounted above a planar waveguide that has been patterned with reflective facets at the focal point of each lens. The facets reflect incoming light into guided modes of the waveguide towards edge-mounted photo-voltaic (PV) cells. This type of concentrator is compatible with traditional solar trackers but its unique geometry allows for more flexibility. By laterally translating the lens array with respect to the waveguide it is possible to couple off-axis light into the PV cell.

In this work I evaluate some different implementations of the planar micro-optic solar concentrator optimized for this type of tracking, discuss a designed and implemented mechanical tracking platform to house the concentrator, and cover the electrical control and feedback used to maintain alignment. I then present some measurements from the system demonstrating functional tracking.

.

Chapter I :

Introduction

I.A Concentrated Photovoltaic Systems

Concentrated photovoltaic (CPV) systems use optical components to concentrate direct sunlight onto photovoltaic (PV) cells. CPV systems trade expensive photovoltaic material for inexpensive glass or plastic optical components such as mirrors or lenses which can reduce the total system cost. Because of this reduction in PV material, CPV systems can leverage expensive multi-junction solar cells to achieve high efficiency and still be economical. Étendue states that the input diameter of an optical system multiplied by the acceptance angle remains constant throughout that system [2]. As the concentration ratio of a CPV system increases its angular acceptance decreases which results in the requirement of tracking mechanics to maintain alignment with the sun. CPV systems come in a large variety of configurations employing different types of concentrating optics, tracking mechanics and PV cells.

Most high concentration (>400x) CPV systems require precise two-axis tracking to maintain alignment with the sun over the course of the day and the year. For example, a 500x CPV system from Concentrix Solar has an acceptance angle of ±0.6˚ [3]. The concentrator array pictured in Figure I-1b is 28.8m^2 and weighs almost 900kg [4]. It is mounted on a common two-

axis tracking platform to maintain normal illumination that is designed to withstand wind loading and frame flexure. The tracking system alone accounts for almost one quarter of the entire system cost.

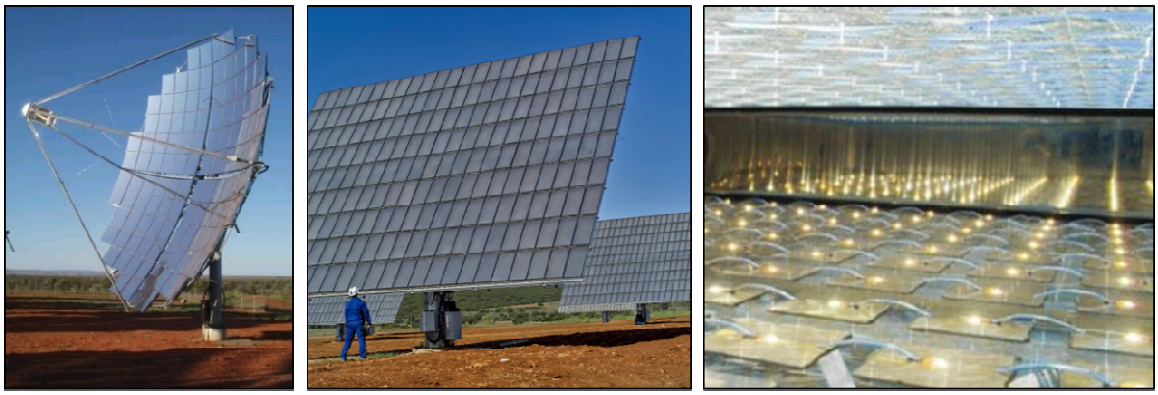

Figure I-1: Some current concentrated photovoltaic (CPV) systems and their tracking mechanics from (a) Solar Systems and (b) Concentrix Solar. (c) Inside view of a Concentrix Solar CPV module. *Images courtesy of Solar Systems and Concentrix Solar.*

As seen in the Concentrix Solar concentrators pictured above, there is a trend in CPV towards segmenting the aperture of the system so that arrays of paired concentrators and photovoltaics are mounted together on a single tracking platform.

I.B Planar Micro-Optic Solar Concentrator

This section describes previous research done by our group, primarily by Jason Karp. In our work on solar concentrators we wanted to keep the aperture segmentation seen in many CPV systems like the Concentrix Solar module above but replace the 1:1 array of photovoltaics with a single PV fed by a common optical output of an array of apertures. The result was the planar micro-optic solar concentrator (PMSC) [1] [5]. The PMSC consists of a micro-lens array mounted above a planar waveguide that has been patterned with reflective facets, or injection

elements, with the same pitch as the lens array. Normally incident light is focused by the lenses in the array through the planar waveguide onto the reflective facets. The facets reflect light into the waveguide where it propagates by total internal reflection (TIR) towards the edge-mounted PV cell.

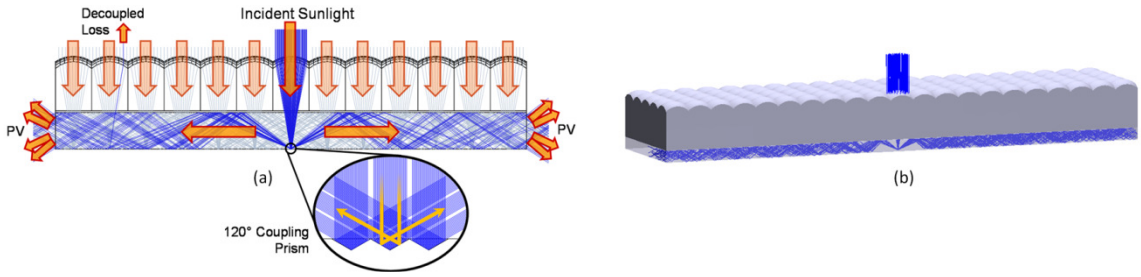

Figure I-2: Illustration of PMSC operation. (a) Incident sunlight is focused onto reflective coupling prisms which inject light into guided modes of a planar waveguide toward edge-mounted PV cells. (b) Perspective view with one lens illuminated.

Another important design constraint for this system was manufacturability. A design with a uniform thickness was chosen for compatibility with inexpensive manufacturing processes such as roll-to-roll processing as opposed to molding which is used in other waveguide concentrators [6] [7].

The current prototype was fabricated in our lab and consists of a hexagonal packed F/3.0 lens array from Fresnel Technologies and a BK7 microscope slide as the planar waveguide. The coupling prisms are molded onto the back of the microscope slide in SU-8 photoresist by a 120˚ prism mold from Wavefront Technology. Next the SU-8 molded prisms are exposed by a collimated ultra-violet (UV) source through the lens array to yield a hexagonal pattern of exposed regions whose size depends on the amount of collimation of the UV source. The molded features are then coated in aluminum and then sonicated in a bath of developer to lift-off the unexposed regions leaving behind an array of reflective facets.

The current prototype was characterized using a Xe arc lamp solar simulator. The efficiency of our current prototype was measured to be 52.3% and the output was effectively

homogenized by the waveguide. In Figure I-4b the simulated efficiency of our current prototype and an optimized singlet design are plotted vs. concentration ratio. As the concentration of the system, which is controlled by the length, increases so does the propagation loss due to a higher chance of subsequent interaction with coupling feature. One solution to decrease the slope of the efficiency vs. concentration curve is to use bypass elements connected to the coupling features that divert light from subsequent interactions with the coupling feature [8]. Ultimately these features will still decouple the light as with each interaction they increase the angle of propagation. This increase in angular spectrum limits possible opportunities for secondary concentration [9].

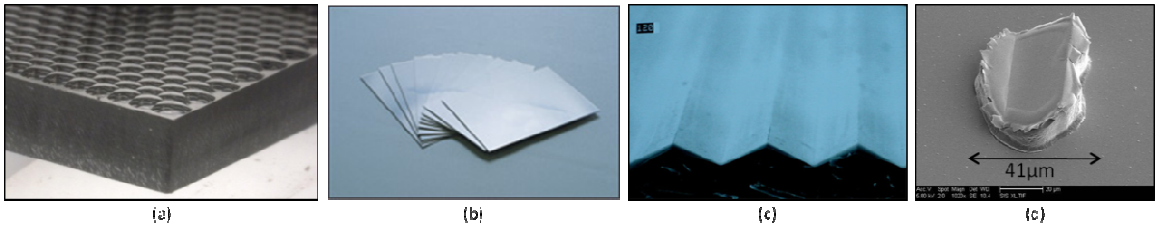

Figure I-3: Components of current PMSC prototype. (a) Hexagonal packed lens array from Fresnel Technologies. (b) BK7 microscope slide for planar waveguide. (c) 120˚ prism mold with 50µm period. (d) Close-up of coupling prism formed in SU-8 photo-resist and coated with aluminum. [5]

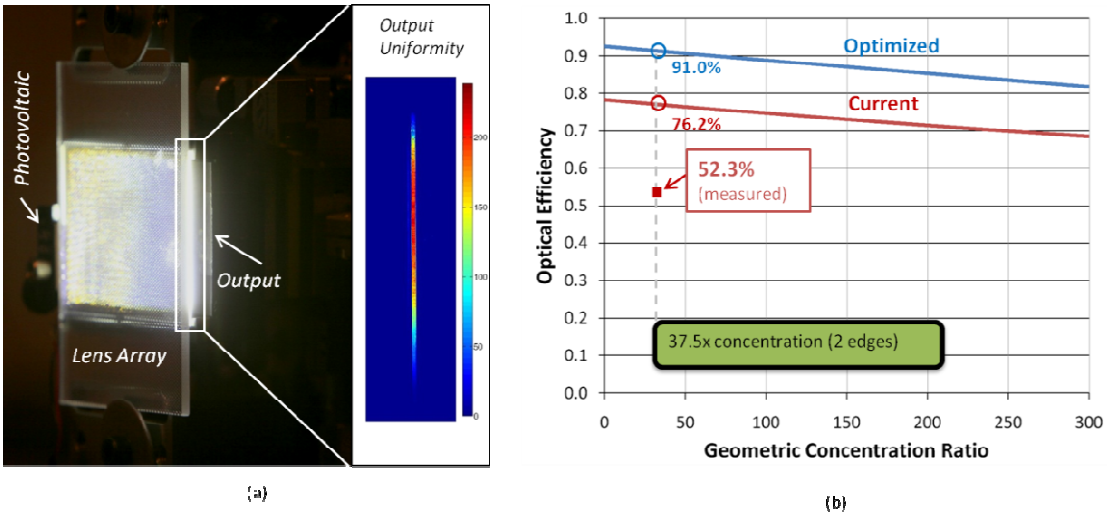

Figure I-4: (a) Current prototype functioning with normally incident light from solar simulator. (b) Simulated curves of optical efficiency of system with current lens and optimized lens with one point of measured data at current concentration. [5]

I.C Tracking with Planar Micro-Optic Solar Concentrator

The PMSC can be used in with a conventional two-axis tracker like those seen in Figure I-1; however its unique geometry allows some flexibility in tracking. For incoming light that is not normally incident, the focal spot moves in the plane of the coupling prisms by a distance F*tanθ. In order to re-couple this light the waveguide can be shifted laterally so that the focal spots fall on the coupling prisms.

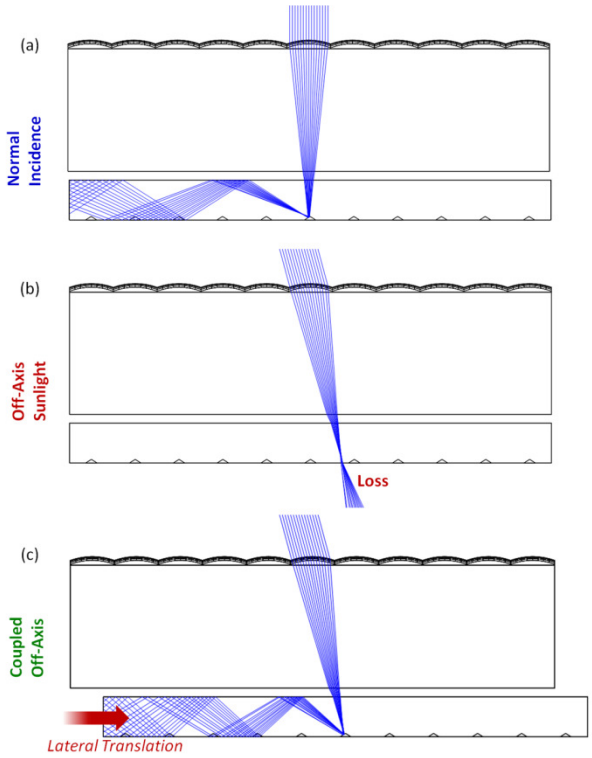

Figure I-5: Illustration of PMSC lateral-translation micro-tracking. (a) Operation of PMSC for normally incident light. (b) Off-axis sunlight results in a different location of focal spot and misses the coupling feature resulting in loss. (c) Lateral translation of the waveguide moves the coupler to the new focus. [10]

This type of tracking is possible with other segmented aperture CPV systems that use arrays of optics and photovoltaics, however since the lateral translation is controlled by the focal length the translations would be much larger. Making a traditional array with focal lengths

similar to what we use in the PMSC would be impractical due to the large number of PV cells that would be required.

Another factor that makes micro-tracking more practical for the PMSC than other segmented aperture systems is that the output is spatially homogenous regardless of the input angle. As light enters a lens off-axis the point of best focus travels not only in the lateral direction but also in the vertical direction. In a system with a PV cell behind each lens tracking the sun with only lateral motion would result in a very non-homogenous illumination of the solar cell unless accompanied by an additional homogenization optic. By choosing a coupler that is as large as the largest focal spot in the desired angle range the PMSC becomes immune to changes in the focal spot across the angular spectrum as all angles are injected into and homogenized by the waveguide.

I.D Thesis Outline

This thesis explores micro-tracking of a planar micro-optic solar concentrator and all of the details: optical, electrical, and mechanical that are required for a well functioning system. To these ends, this thesis is organized as follows:

- Chapter II focuses on optical design and includes a discussion of: the angles of interest for a micro-lens in a micro-tracking PMSC, a design study of different micro-lens designs, design constraints on coupling features and their effect on performance, full concentrator simulations using select lenses from the design study, and experimental verification of ZEMAX simulations.

- Chapter III focuses on mechanical design and includes a discussion of: the implementation of motion used in micro-tracking platform, that implementations

consequences on the tracking algorithm, the design of the micro-tracking platform in SolidWorks, and the fabricated result

- Chapter IV focuses on electronics and includes a discussion of: the micro-controller and development board being used, the motors and motor drivers used, the solar cell and its implementation in the feedback loop, and a circuit diagram showing the interconnection of the electronic components.

- Chapter V covers experimental results from the micro-tracking platform and includes a discussion of: a wide-area search algorithm for initial alignment, the method of push-button alignment of the micro-tracker, a small area x-y scan algorithm with experimental results using solar simulator , a one-axis hill-climbing algorithm with experimental results from using a solar simulator, the modifications to the hill-climbing required for tracking the sun, and experimental tracking results using a two-axis hill-climbing algorithm to track the sun.

- Finally, in Chapter VI I summarize the major contributions of this work and give suggestions for future applications.

- In the two appendices I include my source-code for the micro-controller and provide the lens prescription data from ZEMAX for the micro-lenses in the design study.

Chapter II :

Optical Design for Micro-Tracking

Optical components used in solar concentration have different metrics for performance than optics used in imaging. The importance is not on making a distortion-free image of the sun but rather on making a small uniform spot to illuminate your power generating device. Surface reflections and material absorption are extremely important as they result in loss of potential power. Susceptibility to photo-damage, such as yellowing or loss of mechanical integrity, has to be considered along with index of refraction and dispersion when choosing materials as the optics should last years in the sun with minimal performance degradation.

In a PMSC the optical efficiency of the system is the coupling efficiency multiplied by the propagation efficiency. The coupling efficiency includes Fresnel reflections from surfaces, the area of focal spot with respect to area of coupler, and how well the coupler injects light into guided modes at the given incoming angles. Propagation efficiency includes material absorption and de-coupling from subsequent interaction with coupling features. Maximizing these two efficiencies over a large range of angles is the primary goal of optical design in this section.

II.A Micro-lens Requirements for Micro-Tracking

In order to maximize the coupling efficiency, the lenses used in this type of concentrator with micro-tracking are constrained to have a small spot-size in the plane of interest over a relatively large range of angles. The lenses should be optimized over a range of angles that is weighted by the integrated solar intensity received at those angles. Ultimately the angular spectrum of the solar intensity depends on the role the micro-tracker is taking in the system.

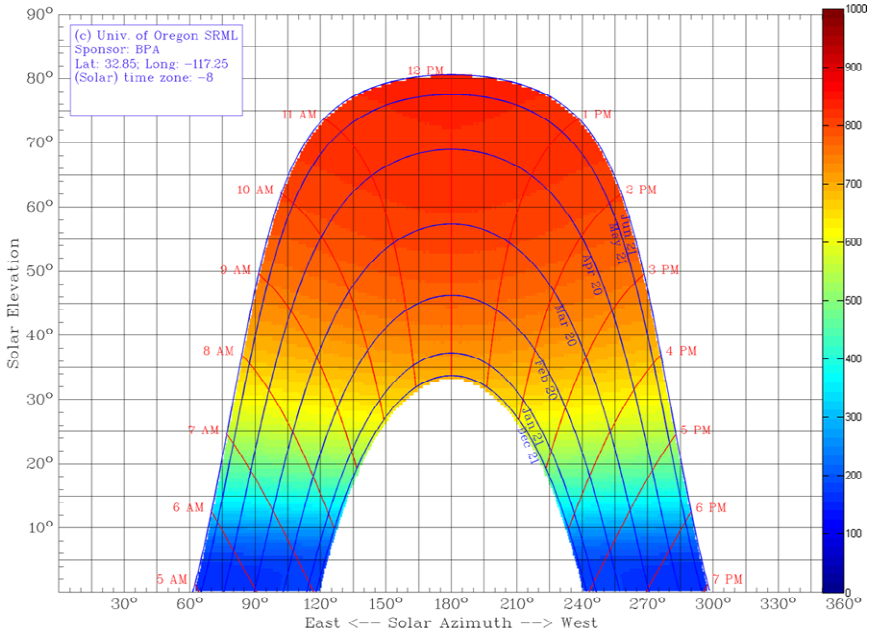

Figure II-1: Plot of path and intensity of sun in San Diego over the course of a year. *Path data courtesy of University of Oregon, Solar Radiation Monitor Laboratory. Intensity plot courtesy of Jason Karp.*

In Figure II-1 above the intensity of the sun is plotted vs. altitude and azimuth here in San Diego over the course of a year. Using that data and including cosθ geometrical losses the intensity vs. angle north-south and angle east-west was plotted in Figure II-2 for the case of a fixed panel mounted at latitude and a panel in a polar tracking system.

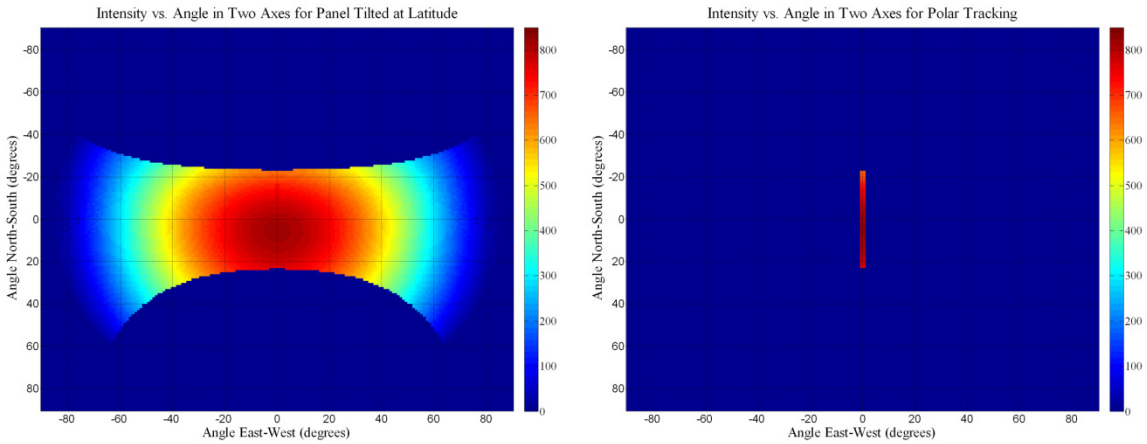

Figure II-2: Plot of intensity of sun over a year with respect to fixed panel mounted at latitude (left) and plot of the intensity of sun with respect to panel in a polar tracking system (right). *Plots courtesy of Katherine Baker.* [11]

For the configuration with no gross-mechanical motion and only two-axis micro-tracking with the concentrator mounted angled at latitude I put my target for a micro-lens to have good performance up to at least 40˚ off-axis. Fixed-panel mounting results in a large reduction in intensity due to the cosine of the angle between the surface normal and the sun.

Another option for this type of system is single-axis polar tracking in addition to micro-tracking. As shown in the figure above, this reduces the required angles for the micro-tracking to only the declination angle of ±24˚ while increasing the possible concentration of and reducing the tolerances of a polar tracker. The cosθ geometrical loss is negligible in this case as compared to the case with no gross mechanical tracking.

II.B Micro-lens Design Study

In the process of searching for micro-lenses to be used several potential candidates were evaluated, each with their own strengths and weaknesses. The optimization for the various configurations mentioned here were done using the ray-tracing program ZEMAX. Optimization in ZEMAX works by using predefined algorithms to find local minimums in a user-defined merit

function, which in this case was RMS spot radius over a range of input angles. The designs covered in this section will be published in an upcoming journal paper [12]. An alternative method to find candidate lenses is to use the Simultaneous Multiple Surface (SMS) algorithm as seen in [13].

The optimization for these lenses was done in the sequential version of ZEMAX as optimization is much faster than in the non-sequential version. The sequential version of ZEMAX requires that the order of interactions with each surface in the optical system be known beforehand which rules out simulating the injection facets or planar waveguide. Because of this it is important to keep in mind how performance of the lens affects the system as a whole. For example if the merit function of the lens optimization puts more weight on effectively focusing larger angles, then the spot size on average will tend to grow. This growth in spot-size has to be accommodated by a larger coupling feature which will tend reduce propagation efficiency, especially in configurations with higher concentration. In this case it must be carefully evaluated whether the increase in angular acceptance and coupling efficiency is offset by reduction in propagation efficiency.

In these simulations hexagonal lenses were used as they can be easily arrayed and make good use of area. The optimization was done over the solar spectrum by defining a list of discrete wavelengths with weighted intensity. Surfaces were defined with anti-reflection coatings which transmit 99.5% of the light and reflect 0.5%; physically achieving good anti-reflection coatings over a broad angular and wavelength range is of great importance to this work but is beyond the scope of this thesis. Acrylic was used for singlets and polycarbonate was used for the second element in optics with multiple components to compensate for dispersion. BK7 was used for the waveguide.

II.B.1 Refractive Singlet Micro-lenses

The current prototype is not an optimized lens but rather one of the best that was commercially available for on-axis performance in a PMSC. As you can see in Figure II-3, the performance falls off drastically after 20˚. In Figure II-4 a refractive singlet optimized for performance up to 25˚ is shown. This micro-lens has better performance at larger fields but is ultimately a singlet cannot work well over such a large range in field angles and wavelengths.

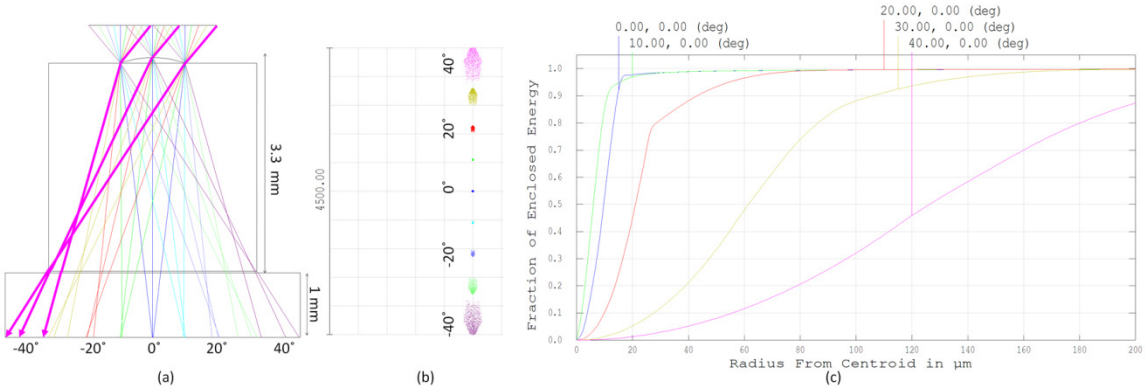

Figure II-3: Characterization of current prototype refractive singlet lens. (a) Layout of lens with rays traced from fields -40˚ to 40˚ in 10˚ increments. (b) The focal spots resulting from those fields. (c) Fraction of enclosed energy as a function of radius from centroid for those fields.

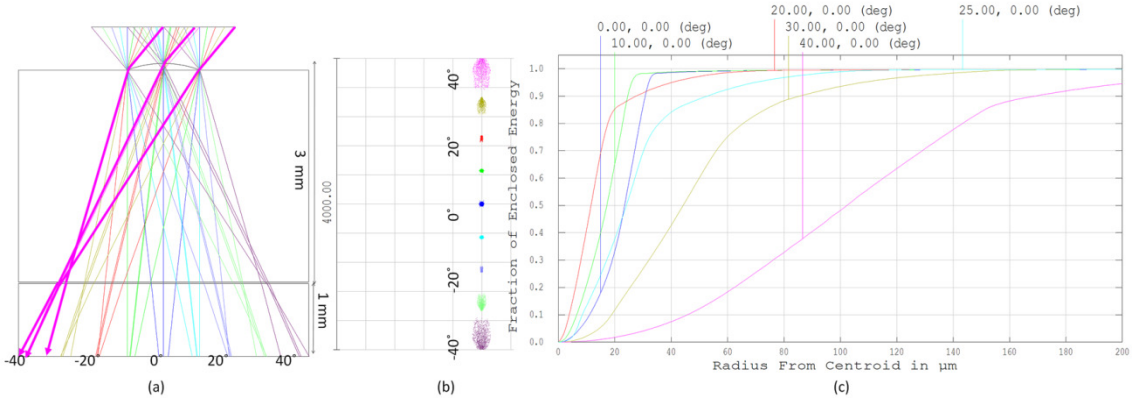

Figure II-4: Characterization of refractive singlet optimized over 24˚. (a) Layout of lens with rays traced from fields -40˚ to 40˚ in 10˚ increments. (b) The focal spots resulting from those fields. (c) Fraction of enclosed energy as a function of radius from centroid for those fields.

II.B.2 Refractive Doublet Micro-lens

Next, a doublet micro-lens was optimized to work well over a range of ±35˚. Typically when optimizing this class of micro-lens for a large field of angles, the solution vignettes angles higher than the largest angle input into the optimization. That is at input angles higher than this the light is no longer focused correctly as it travels into a neighboring secondary lens. This is because the hardest constraint to meet on the optimization is that the first lens must have enough power at the highest angle of interest such that the rays enter the corresponding secondary lens and are not vignetted. This type of system works better to focus light than the singlet but has the downsides that it's more complex to fabricate, has more surface reflections, and can have a hard-cutoff where it almost entirely ceases to concentrate due to vignetting and TIR at the first lens-air interface.

The lenses that comprise this doublet are constrained to move together for simplicity. Not constraining the lenses to move together would increase complexity but would allow result in higher achievable concentration and an angular range less limited by vignetting [13].

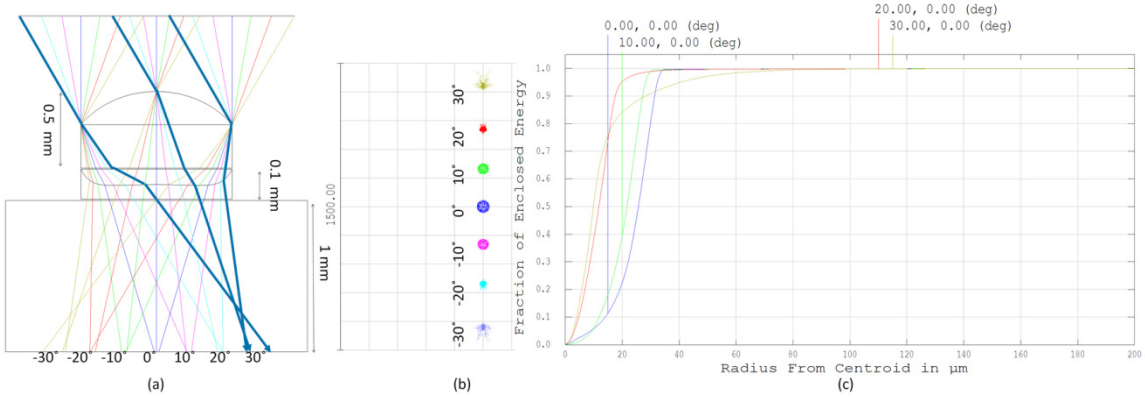

Figure II-5: Characterization of refractive doublet optimized over 30˚. (a) Layout of lens with rays traced from fields -30˚ to 30˚ in 10˚ increments. (b) The focal spots resulting from those fields. (c) Fraction of enclosed energy as a function of radius from centroid for those fields.

II.B.4 Reflective Micro-Lenses

Reflective micro-lenses offer the benefit that their spectral performance is less constrained than a refractive lens because the optical power is more a function of the curvature of the mirror than the index of refraction. One possible downside is that diffuse light is not concentrated and is not transmitted; in a refractive system that transmitted light has the potential to be collected by an existing flat-panel PV device.

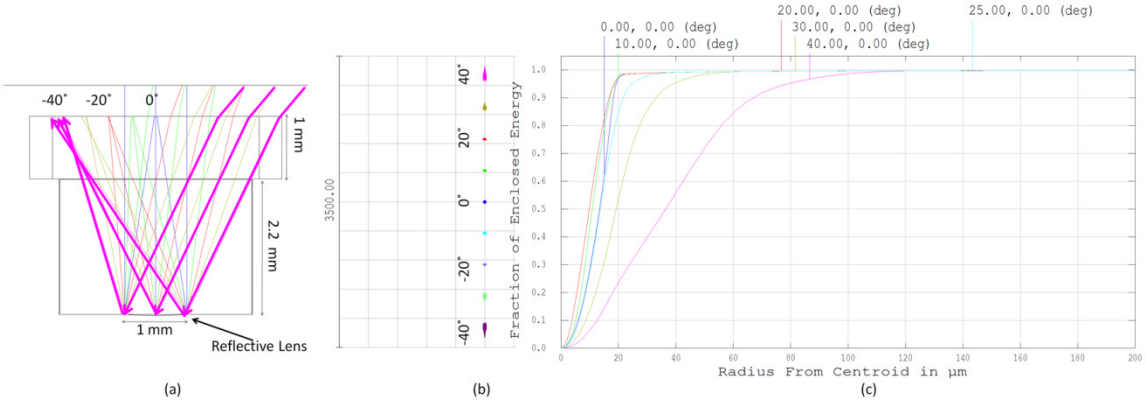

Figure II-6: Characterization of reflective lens optimized over 24˚. (a) Layout of lens with rays traced from fields -40˚ to 0˚ in 10˚ increments. (b) The focal spots resulting from those fields. (c) Fraction of enclosed energy as a function of radius from centroid for those fields.

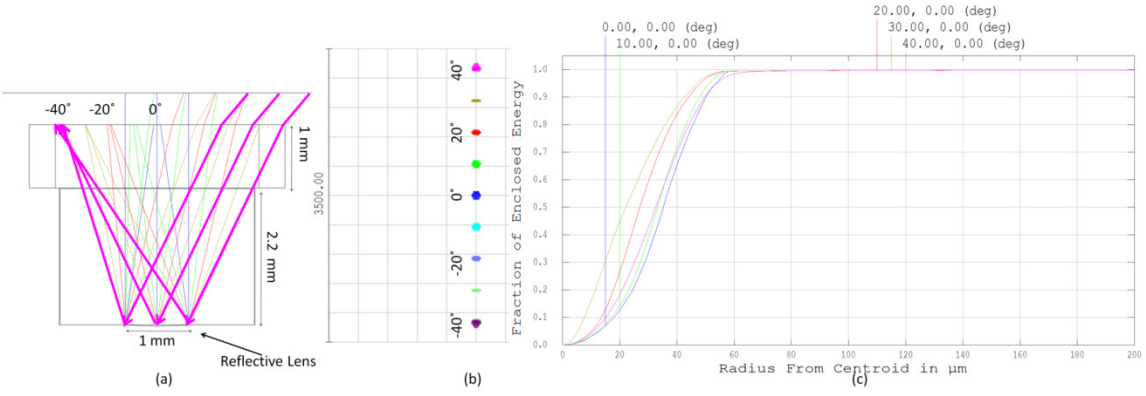

Figure II-7: Characterization of reflective lens optimized over 40˚. (a) Layout of lens with rays traced from fields -40˚ to 0˚ in 10˚ increments. (b) The focal spots resulting from those fields. (c) Fraction of enclosed energy as a function of radius from centroid for those fields.

II.B.5 Catadioptric Micro-lens

This type of lens which combines a refractive and a reflective element have been evaluated as PMSC micro-tracking lenses as well and offer promise. The challenge in this configuration is vignetting of large angular fields if the refractive and reflective are stationary and the waveguide moves with respect to them. If both sets of lenses were allowed to move independently it would relax this constraint but add complexity. Also, due to the large amount of interfaces encountered, surface reflections would likely take a toll and anti-reflection coatings would be extremely important.

II.B.6 Review of micro-lenses

The singlet refractive micro-lenses are the easiest to fabricate and control and have the worst performance. These types of lenses are more suitable for a PMSC with moderate concentration along with a single-axis polar tracker. As concentration increases the additional propagation losses due to larger couplers would offset the benefit of simplicity.

Doublet micro-lenses are more difficult to fabricate and experience more surface reflections than singlets but offer smaller spot-sizes at higher field angles. When each lens in the doublet is not allowed to move independently vignetting becomes a problem at large input angles. Performance can be enhanced and vignetting can be eliminated by allowing independent motion of each lens, but this performance increase must be weighed against the increased cost complexity.

Reflective micro-lenses have excellent performance across a wide spectral-band as their performance is more controlled by the curvature than by the index of refraction. These types of lenses could not be used in a PMSC mounted on top of an existing flat-plate PV system. As seen

in Figure II-6 and Figure II-7 above, angular acceptance can be traded for spot-size to tailor the lens to specific requirements set by whether the system will be tracked or not.

Catadioptric micro-lenses have the potential for good performance over a large range in angles but suffer from the same problems with vignetting and surface reflections as doublet micro-lenses. The extra complexity and surface reflections would have to be compensated by extremely small spots over the field to be economically worth it. If such a lens was designed that achieved extremely small spot-sizes but suffered significant surface reflections it could still be useful in a PMSC with high concentration as the magnitude of slope of the optical efficiency with respect to concentration would be decreased. Ultimately the choice of micro-lens in a micro-tracking PMSC must consider angular acceptance and spot size as well as cost, complexity, and ease of fabrication.

II.C Coupling Feature Performance

Along with the lens the coupling feature is of critical importance to the function of the PMSC. In order to work well in a micro-tracking system the coupling feature must inject light into guided modes over a large range of input angles to maximize coupling efficiency, but also have a small footprint to minimize secondary interactions in order to maximize propagation efficiency.

Figure II-8 below plots the percentage of light that reaches the output PV cell when light from an incoming angle is incident on the face of waveguide. The regions of low or no coupling are due to double bounces as seen in the figure or the case where the incoming angle would be back reflected by a near perpendicular facet. The area of low coupling is due to the percentage of light that hits the outside faces of the coupler as opposed to internal faces. The area of no

coupling in the middle of the graph corresponds to the case where light comes in perpendicular to the direction towards the PV and does not TIR off of the side-wall.

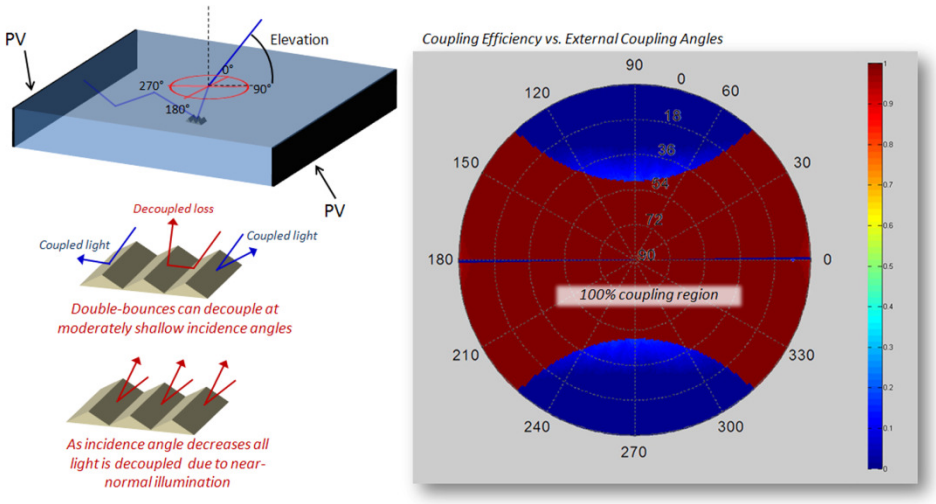

Figure II-8: Figure illustrating wide angle function of coupling features. Plot (right) shows coupling efficiency vs. external angles (not including lens NA) for 120˚ prism.

Another variable that must be considered in a properly optimized system is the coupler area. Large coupler areas loosen the requirement of the lens to create a small spot over a large angular field but increase propagation loss as there is an increased chance of secondary interaction with the coupler which acts to decouple the light.

As mentioned in the introduction chapter, another possibility to improve the coupler performance is to use a more complex structure that is not constrained to be formed from a continuous periodic master. If different couplers can be fabricated as a function of position in the waveguide then they can be tailored to minimize propagation loss by adding bypasses, as in [8], or by tilting slightly in the direction orthogonal to the direction of periodicity in order to minimize interaction with subsequent couplers.

II.D Total PMSC Micro-Tracking Performance

II.D.1 Simulation with Optimized Coupler Sizes

In order to evaluate the optical performance of various lenses in a micro-tracking PMSC system, they were simulated in the non-sequential version of ZEMAX [12]. In these simulations the coupler size was optimized over the range of reasonable performance for each lens. The resulting plots of efficiency vs. angle, seen below in Figure II-9, demonstrate the differences between the prototype singlet, the optimized singlet, and the optimized doublet micro-lenses.

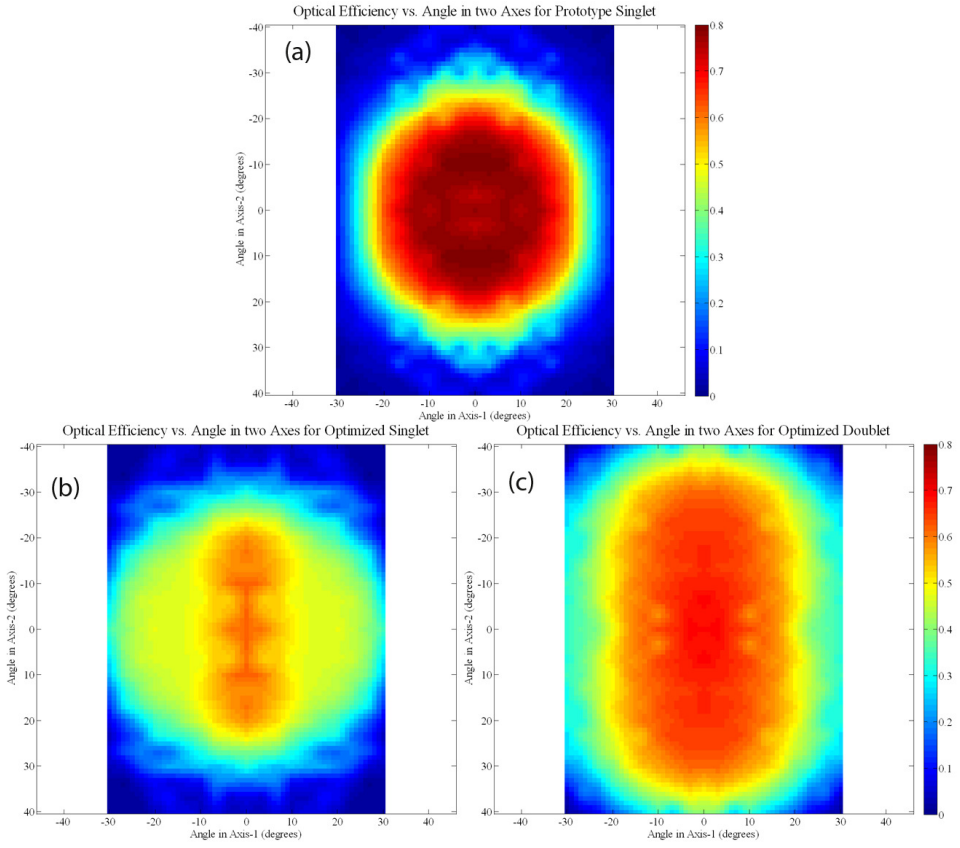

Figure II-9: Plots of efficiency of micro-tracking PMSC over two orthogonal angles for 38x concentration and coupler sized optimized for maximum angular performance for (a) the singlet lens used in the current prototype, (b) a singlet optimized for performance over 25˚, and (c) a doublet optimized over 35˚.

The prototype singlet performed the best on-axis, as expected, and performance fell drastically after 20˚. This lens, or one very similar, could reasonably be used in a micro-tracking system in conjunction with a polar-axis tracker. The optimized singlet demonstrates that when pushed to large angular fields, absolute performance over the entire field is sacrificed. A singlet refractive micro-lens is not able to effectively perform over a large angular and wavelength range while maintaining a relatively high efficiency.

The doublet micro-lens has lower on-axis efficiency than the prototype as a result of increased surface reflections. However, as concentration increases, the performance of the doublet would overtake the prototype singlet as the total efficiency would depend more and more on propagation efficiency. The asymmetrical drop in performance seen here is a result of the asymmetrical performance of the coupling feature rather than the micro-lens. This system could be used in a mechanically fixed system with axis two oriented east-west. One of the more promising lenses seen in the sequential section earlier has not yet been modeled in non-sequentials at the time of this publication; it will be included in [12].

II.D.2 Experimental Verification of Micro-Tracking Simulations

In order to experimentally verify ZEMAX simulations of micro-tracking I fabricated a new PMSC with larger facets, 60µm diameter instead of 40µm, by decreasing the collimation of the UV exposure source. I mounted this PMSC on a rotation stage and illuminated it with a Xe arc lamp solar simulator. The lens array position was controlled with respect to the waveguide by a manual x-y translation stage. After each step in rotation the position was changed to optimize the output current from an edge-mounted PV cell. The performance plotted over angles perpendicular and parallel to the prism direction in Figure II-11 below. In the same figure the results from a ZEMAX simulation that matches the coupler size and fabrication results is

overlaid. The agreement between the simulation and experimental results gives me confidence that the ZEMAX simulations are accurately modeling real world performance.

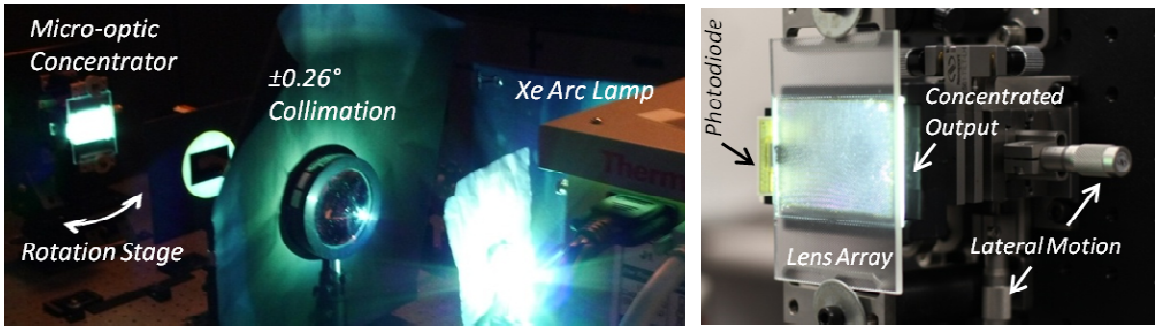

Figure II-10: Experimental lab setup for micro-tracking.

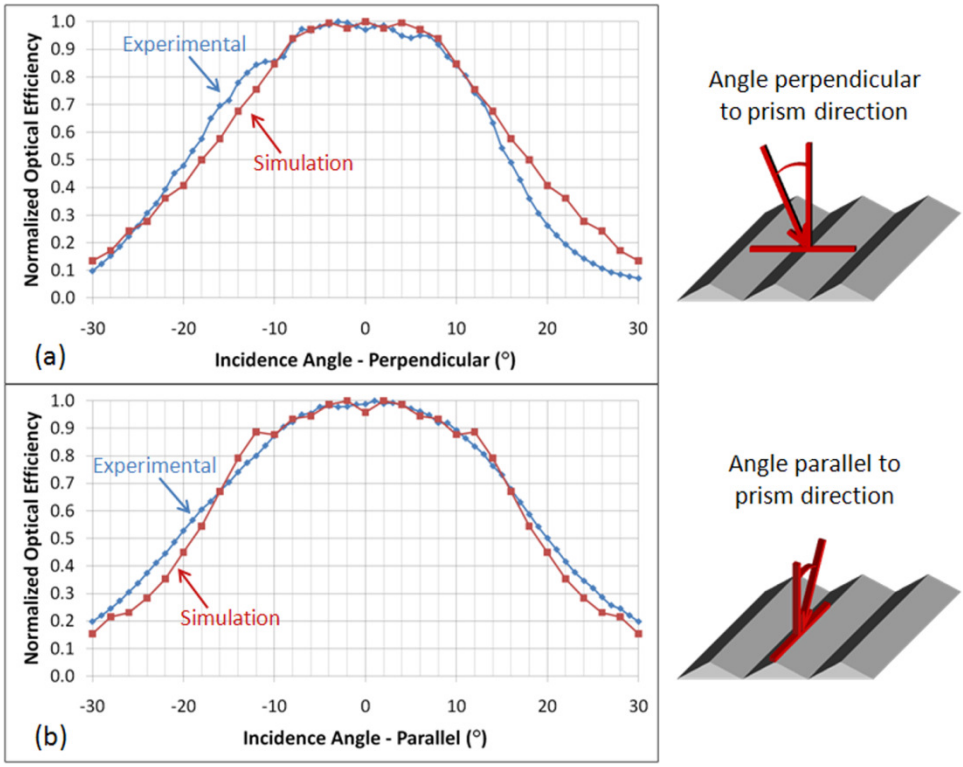

Figure II-11: Plots of normalized optical efficiency vs. incidence angle for angle (a) perpendicular and (b) parallel to prism direction.

Chapter III :

Mechanical Design of Micro-Tracking Platform

The primary role of the micro-tracking platform is to house the concentrator and precisely rotate and translate the lens array with respect to the planar waveguide with electrical control.

III.A Mechanical Actuation

The most selective requirement with respect to the mechanical actuation of the lens array with respect the waveguide is that not only must relative translation be controlled, but relative rotation as well. This requirement rules out more straightforward options that move on rails or tracks.

Our solution was to use three eccentric cams to achieve translation and rotation of the lens array with respect to the waveguide. An eccentric cam is a disc with a center of rotation that is not at the center of the disc. The lens array is held in contact with the cams by small springs. By rotating a cam the point of contact between the cam and the lens array is moved closer or further from the center of rotation. The distance between the two furthest points of contact is

equal to two times the amount of de-center. The maximum required translation in a micro-lens system is the pitch of the lenses, however utilizing only this amount of translation would require discontinuous jumps in position and would complicate the tracking algorithm. For this reason I chose 2mm of de-center for a total of 4mm of translation to accommodate a large angular range for my PMSC with a focal length of approximately 3mm.

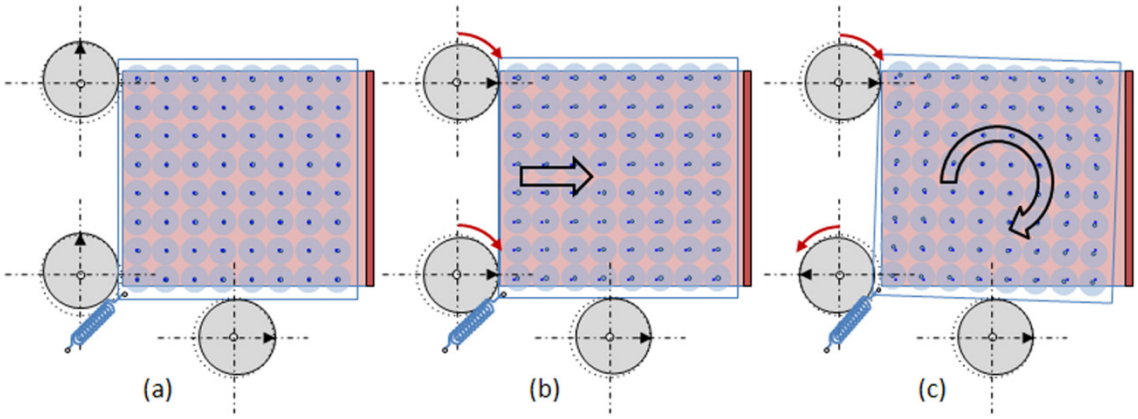

Figure III-1: Figure illustrating how de-centered cams work to accomplish lateral motion and rotation. (a) Intial position, (b) Lateral translation in one axis, (c) Rotation.

The two eccentric cams shown on the left in the Figure III-1 above control both rotation and translation of the lens array with respect to the waveguide. When the axes of the two cams are perfectly aligned and they rotate in the same direction, pure x-axis translation is achieved. When the axes of the two cams are approximately rotationally aligned and they rotate in the same direction the motion consists of mostly translation but some rotation as well. This effect is seen in Figure III-2 where the axes of the two cams are offset by 10˚. The rotation seen is a result of the different slopes of the sinusoidal curves at that particular step. The amount of translation of the contact point for each cam is controlled by a sinusoid so if one of the cams is in the quasi-linear region and the other is near a peak or valley (where the magnitude of the slope decreases) more rotation will be incurred.

This linked rotation and translation is a difficulty that must be overcome in any tracking algorithm using this type of mechanical actuation. One way it can be overcome is by knowing the precise position of each cam and using a lookup table to move to the desired position and rotation. In the current mechanical tracking platform I am using motors without encoders and as such have no knowledge of the precise absolute position of each cam. My method to overcome this difficulty is discussed in the following chapter.

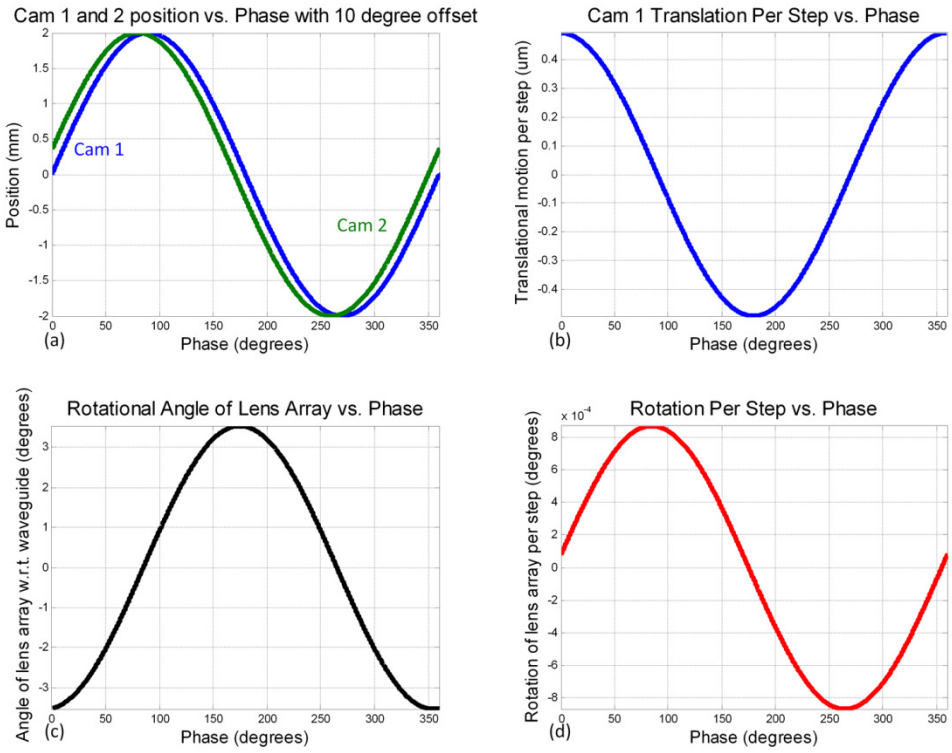

Figure III-2: (a) Contact position of 2 cams as a function of phase of cam. (b) Change in contact position per motor step or resolution per phase of cam. (c) Rotational angle of lens array vs. phase given 10˚ of cams and 5.65mm distance between cams. (d) Change in rotation per motor step vs. phase of cam.

The required resolution in motion depends on the size of the coupling feature. In the current prototype the coupling features were fabricated to be 60µm. From this information I set the target resolution to be at least 5µm per step. In order to accomplish this and maintain a thin panel-like appearance I chose a miniature stepper motor, the ADM1220 from Faulhaber, which

has 20 steps per rotation with ±5% accuracy in each step with an attached 64:1 reduction gear head. The motor and gear head drive a worm drive with a 20:1 reduction that directly controls the eccentric cam. This combination yields 25,600 per rotation of the eccentric cam, or 0.014˚ per step. Because the contact position with the lens array is a sinusoidal function with respect to the rotational phase of the cam the change in contact position varies for each step. As seen in Figure III-2b the maximum amount of change in contact position per step is 0.5µm, which is well within the targeted resolution.

III.B CAD Modeling in SolidWorks

I designed the micro-tracking platform in SolidWorks with the constraint that it must be thin relative to its length and width to maintain a panel-like appearance. Seen in Figure III-3 are the parts that were selected and purchased including the motor and gear-head, the worm and worm gear, and a bearing with the same inner diameter as the worm and worm gear. In Figure III-4 are the various components of the micro-tracking platform that were designed in SolidWorks including the eccentric cam, a coupler that connects the gear-head shaft to the worm and fits into a bearing, the platform bottom, mounts for the motor and worm drive coupler, and a plastic shim that mounts to the platform cover to keep the micro-lens array in contact with the platform bottom. Figure III-5 shows various views of the assembled system with the solar cell attached.

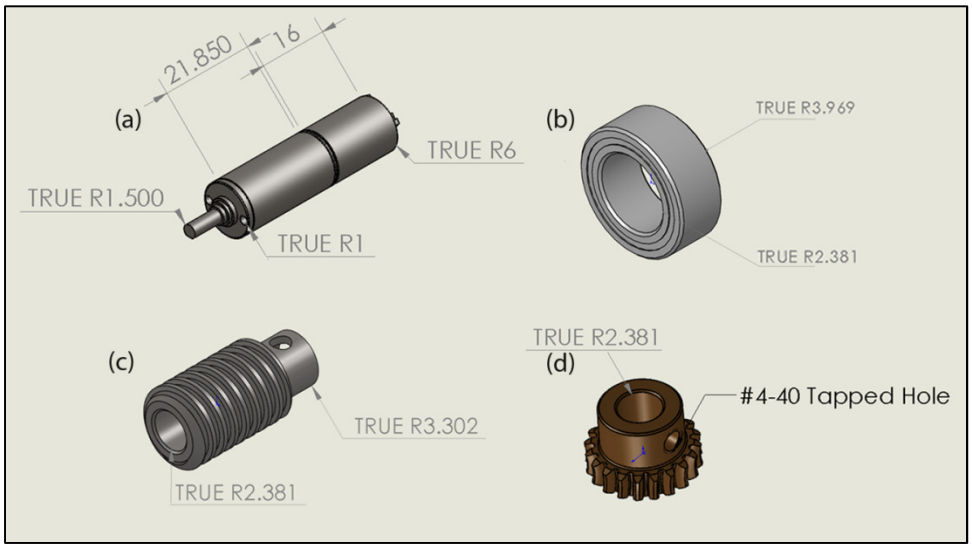

Figure III-3: Selected parts that were purchased. Lengths in mm. (a) Micro-stepper motor from Faulhaber. (b) Bearing used with cams and worm-drive "coupler". (c) Worm driven by motor that drives (d) worm gear that drives cam.

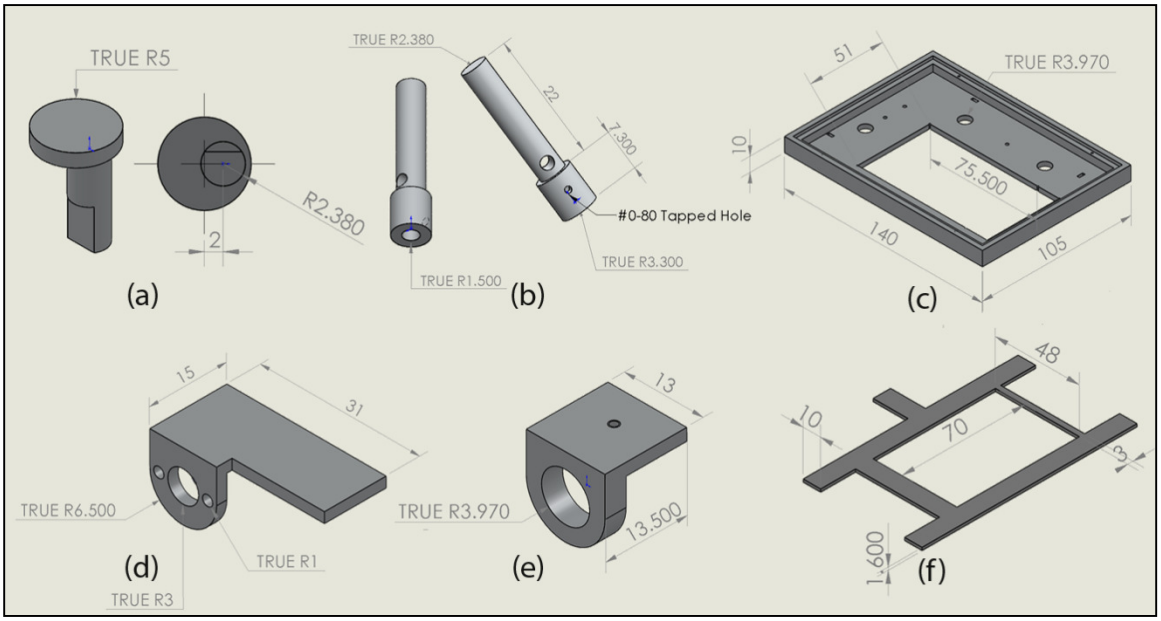

Figure III-4: Designed and fabricated parts. Lengths in mm. (a) Eccentric cam with diameter of 1cm and de-center of 2mm. (b) Worm-drive "coupler", connects motor shaft to worm. (c) Platform bottom, waveguide and solar cell attached via optical adhesive. (d) Motor mount. (e) Worm-drive "coupler" mount. (f) Plastic shim that attached to platform top that keeps lens array in contact with platform bottom.

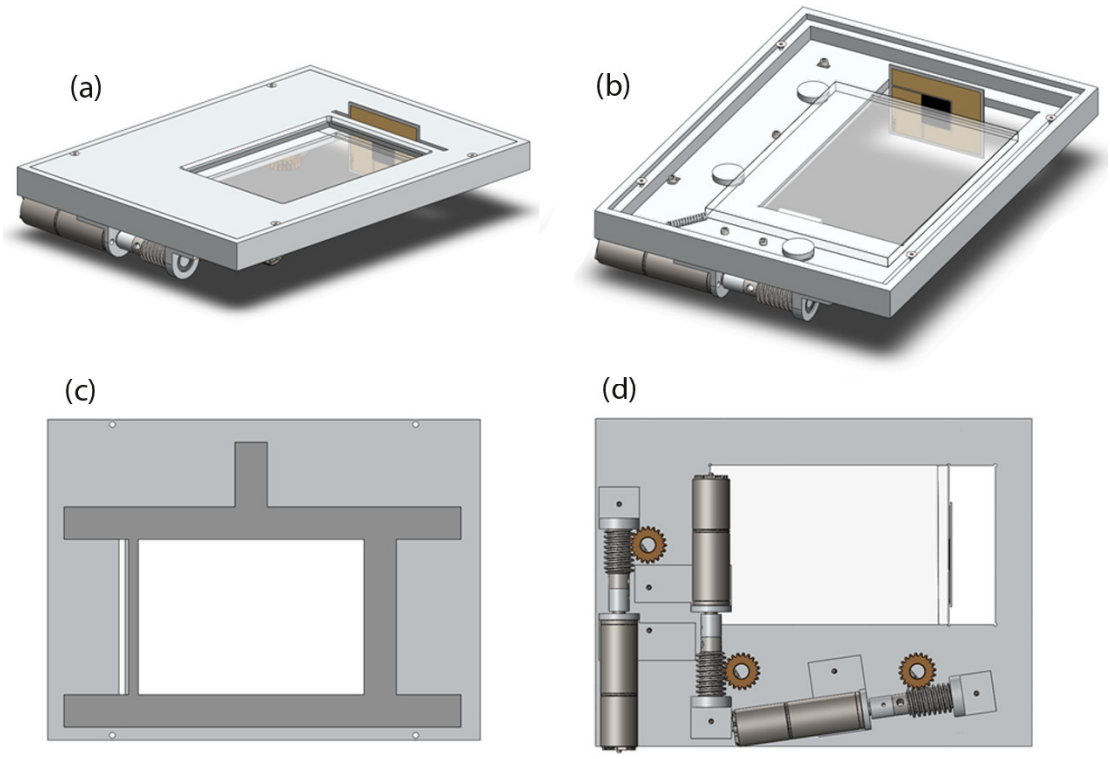

Figure III-5: Assembled parts. (a) Assembled PMSC micro-tracking platform. (b) Assembled platform without cover. (c) Bottom view of platform cover with attached plastic shim. (d) Bottom view of platform with attached motors and worm drives.

III.C Fabricated Platform

After the design process, the parts were fabricated at the SIO machine shop. Aluminum was used as the material and was anodized to reduce friction with the moving lens array. Seen below, Figure III-6, is the end result. The waveguide was mounted by placing the platform upside down and supported by a block smaller than the inside lip but larger than the aperture on the bottom. A thin spacer, the size of the desired airgap was then placed in the gap where the waveguide would go. The microscope slide patterned with facets was then placed on the spacer and glued into place with optical adhesive. The solar cell was attached to a small aluminum

block just the width of the space and the block was attached to the internal sides of the platform using optical adhesive.

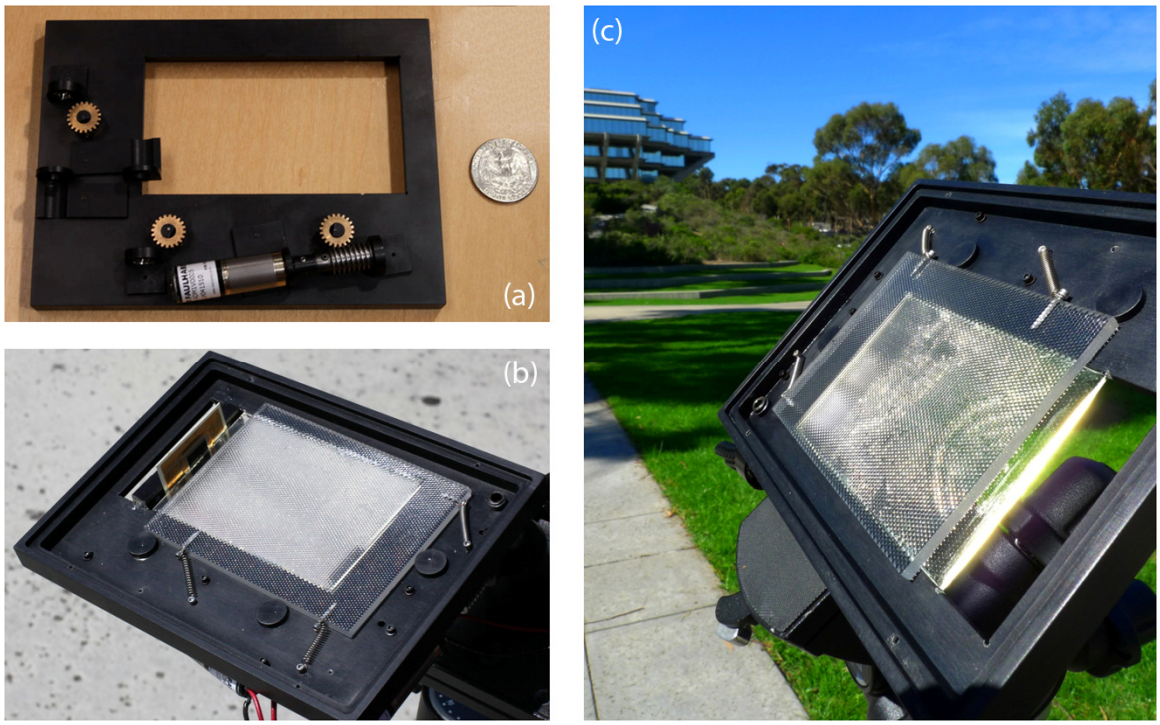

Figure III-6: Figure showing fabricated system. (a) Bottom view of partially assembled micro-tracking platform. (b) Top view with attached solar cell. (c) System without solar cell demonstrating bright output, same as image used in OPN article [14].

Chapter IV :

Electrical Design

In this section, the electrical control and feedback of the micro-tracking platform is discussed. The purpose of these electronics is to be able to measure the output from the solar cell and, using the mechanics from the previous chapter, adjust the lateral position and rotation of the lens array with respect to the waveguide in order to maximize the output from the solar cell.

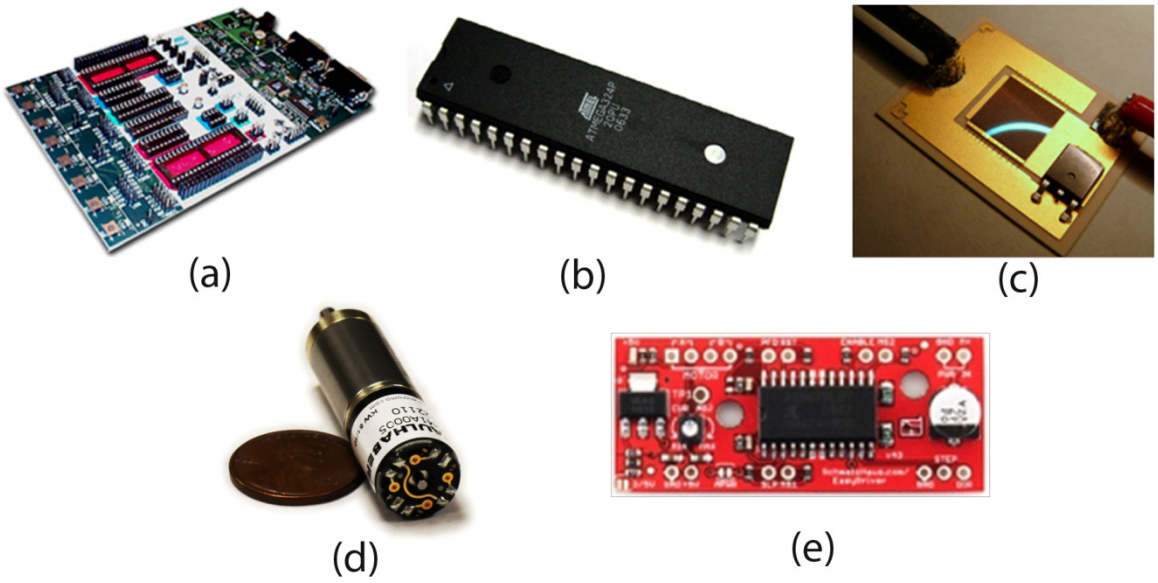

Figure IV-1: Electronic components used in micro-tracking platform. (a) STK-500 Development board. (b) ATmega324p micro-controller. (c) Cyrium multi-junction solar cell. (d) Faulhaber miniature stepper motor ADM-1220 shown next to penny for scale. (e) EasyDriver stepper motor driver. *Images courtesy of Atmel, Sparkfun, and Cyrium Technologies.*

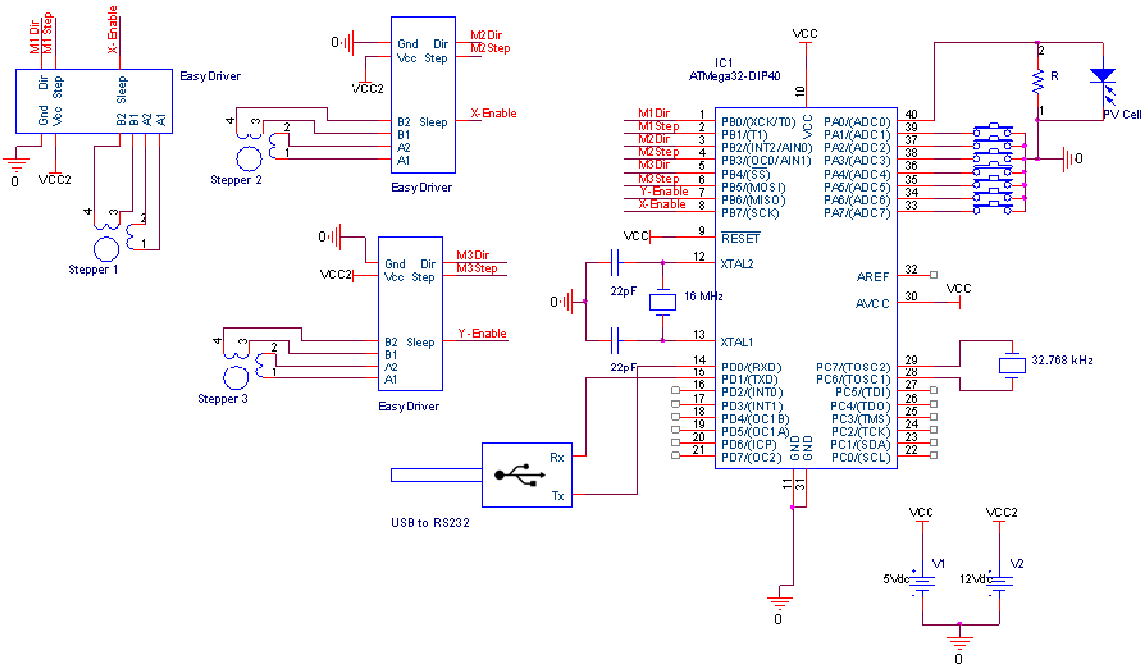

Figure IV-2: Electrical schematic showing connection between various electronic components used in micro-tracking platform.

IV.A Micro-controller

Instead of using a laptop to control the micro-tracking platform I decided to use a micro-controller to better emulate what could be used in an actual deployed system. The micro-controller I chose was the ATmega324p. I chose this micro-controller for its large number of general I/O ports for controlling the motors and receiving user input, its A/D converter for measuring the output from the solar cell, and its onboard UART (serial) port for data-logging. I chose the STK500 development board to program the micro-controller. This development board has an onboard programmable voltage regulator as well as push-buttons and LEDs that greatly assist in prototyping.

IV.B Motors

As mentioned in the previous chapter, I chose the ADM1220 miniature stepper motor from Faulhaber to control the rotation of my eccentric cams. I chose this motor for its small form factor as well as low drive requirements. The version of the ADM1220 I chose nominally requires 3V for voltage mode operation and 0.2A for current mode operation.

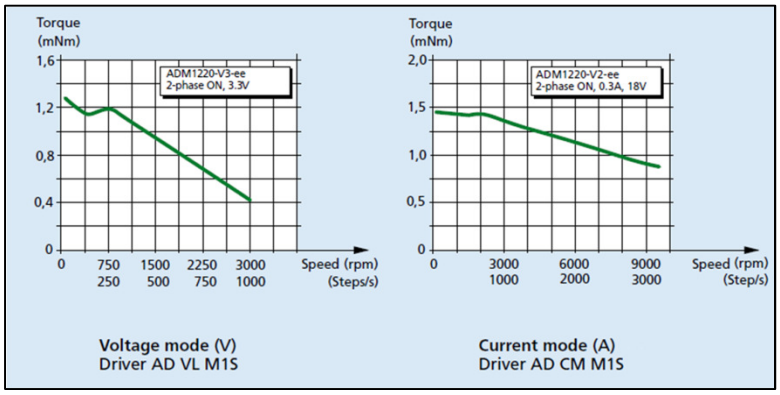

Figure IV-3: Stepper motor torque vs. rpm when driven with a voltage mode (left) and current mode (right) drivers [15][14].

In Figure IV-3 above the stepper motor torque is plotted vs. rpm for a current mode driver and a voltage mode driver. Stepper motors are controlled by the magnetic field created when current flows through their coils. Voltage mode drivers simply apply a voltage across the coils of the motor and the steady-state current that flows is dependent on their series resistance. Voltage-mode drivers are often used because of the simplicity of their implementation. Their downside, as demonstrated in the figure above, is that their performance is limited at higher speeds. This limitation is due to the inductance of the motor coils which causes a non-zero rise-time to the steady-state current when the state is changed.

Current-mode drivers apply a voltage typically 5-6 times the nominal voltage across the coils of the motor in a PWM fashion to create a constant current flowing through the coils. These

types of motor drivers achieve a higher torque for a given RPM but are generally much more complicated. I chose the EasyDriver, Figure IV-1e, breadboard-able current-mode driver that requires no external circuitry in order to simplify the operation of the stepper motors. To control the motors I use three pins: the step pin which advances the state of the motor when given a pulse from the micro-controller, a pin that controls the direction by sending either a high or low voltage from the micro-controller, and a sleep pin that disables the current flow when held low. The EasyDriver has a potentiometer to control the current flowing through the coils. I use higher than nominal current in order to achieve a high speed without missing any steps. The duty-cycle of motor operation is very low which allows me to use this high current and disable the current when not rotating the eccentric cam. The mechanical detent of the motor and gear-head prevents motion when current is not flowing.

IV.C Solar Cell

The solar cell used in the micro-tracking platform was a high efficiency multi-junction CPV cell from Cyrium Technologies shown in Figure IV-1c. In this system it is used as a feedback mechanism to control the alignment of the lens array with respect to the waveguide. For these purposes, the current from the cell is fed through a resistor to create a voltage that can be measured by the ADC onboard the micro-controller. This implementation functions well as long as the voltage stays within the linear region of the cell. A more robust, but not currently required, implementation would use the solar cell along with a transimpedance amplifier for more linear results across a greater range.

Chapter V :

Experimental Results from Micro-Tracking Platform

V.A Initial Alignment

Initial alignment, whether manual or with a search algorithm, is accomplished using alternating translation and rotation of the lens array with respect to the waveguide. The output from a rotationally misaligned PMSC exhibits a broad curve with a low-valued peak when the lens array is translated laterally. In contrast, a rotationally aligned PMSC exhibits a narrow curve with a high-valued peak under the same circumstances. In order to find the maximum output the lens array is first rotationally misaligned to broaden the "translational" peak and make finding it easier. After the "translational" peak is found, the lens array is iteratively rotated and translated to find the total peak.

The lack of positional feedback, mechanical backlash, coupled rotation and translation of one axis, large search area, and possible intensity changes due to cloud cover make creating a search algorithm with an unknown initial cam position difficult. The lack of positional feedback can be overcome by counting steps and always returning to a known home position, however this solution is not robust as it depends on the motors never missing a step. Including positional

feedback into the system with encoders, contact switches or Hall-effect sensors with small magnets would be the optimal solution. Mechanical backlash can be quantized and calibrated for in the algorithm such that counting of steps can be relatively accurate. Using a lookup table to find the approximate direction would reduce the search area, but requires knowledge of time, location, and orientation of the micro-tracking platform. Another possible solution to the search area problem is to mount a low-resolution CMOS sensor behind a section of micro-lenses and use the location of the focal spots to find the approximate direction to the sun. To solve the problem of intensity changes due to cloud cover, a photo-diode could be mounted on the top cover of the micro-tracking platform that would assist in normalizing intensity data gathered through the PV cell. Without these additions to the micro-tracking platform a simple wide-area search algorithm is difficult and is a problem more suited to a person with a controls background. Future research inside our research group will focus on this topic. The PMSC was manually aligned using push-button input into the micro-controller in the experiments discussed below.

The procedure for aligning by hand using push-button input is straightforward and can be accomplished in less than a minute regardless of initial position using the light scattered from illuminated coupling features. When the PMSC is rotationally misaligned there are small regions which are in alignment due to the periodic nature of the array and the small pitch. By intentionally rotationally misaligning until a small-spot is aligned and then rotationally aligning while keeping the spot centered by translating in the two different axes alignment is achieved. After the system is approximately aligned I use an oscilloscope and the push-buttons to maximize the output.

V.B Alignment Maintenance Algorithms

V.B.1 X-Y Scan

One method to track the sun once it is approximately aligned is to use a similar algorithm to that used in the initial alignment, only search in a much smaller domain. Since the search domain is small, and initial rotation alignment is already achieved, this algorithm only translates the lens array with respect to the waveguide to find the peak output. By choosing a repetition rate based on the width of the peak and how quickly the sun moves, the peak can be found by first finding the peak in one axis, then finding the peak in the other axis, rather than scanning a grid which can be time consuming.

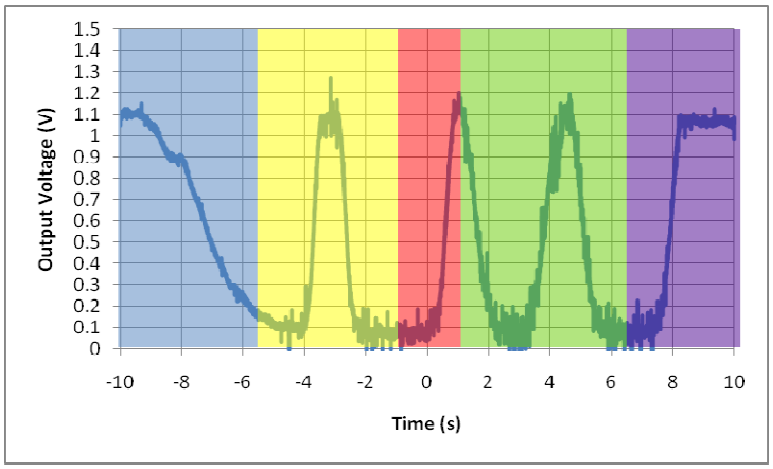

Figure V-1: Result from X-Y scan algorithm. The colored regions from left to right are: intentional misalignment, scan over range in first axis, return to peak found in first axis, scan over range in second axis, return to peak found in second axis and stop.

In order to test this algorithm the micro-controller was programmed and connected to the micro-tracking platform mounted on a digital rotation stage and illuminated by a Xe arc lamp solar simulator. Figure V-1 demonstrates the different phases of the algorithm. The first phase, colored in blue, is the changing output due to rotational misalignment with respect to the solar

simulator created by the rotation stage. The second phase, colored in yellow, scans the position along one axis and records the position of maximum output. The third phase, colored in red, returns to the peak found in the first axis in two steps to account for unknown mechanical backlash. The first step translates the majority of the distance back, and the second step uses a hill-climbing algorithm where the position is advanced as long as the output does not decrease. The next two phases, colored in green and purple, are analogous to phase two and three for the second axis. The X-Y scan algorithm is time consuming and is more suited to occasional re-alignment than alignment maintenance.

V.B.2 Hill-climbing Algorithm

Another algorithm that I explored to maintain alignment with the sun was a simple hill-climbing algorithm. Since the sun is moving in one direction, except for a change in direction in altitude at noon, points in the x-y plane not in the direction of the motion of the sun can be discounted. Alignment can be maintained by moving in one direction in each axis which eliminates the problem of mechanical backlash. The hill-climbing algorithm periodically advances the position in each axis until a decrease in the output voltage is measured. How often the algorithm is run depends on how quickly the source is moving relative to the micro-tracking platform. The position will be advanced at least one step for each run and if the algorithm is run too often it may overshoot the peak and require an x-y scan to reacquire alignment. If it is not run often enough the output will noticeably fall from the peak intensity and the average output will decrease.

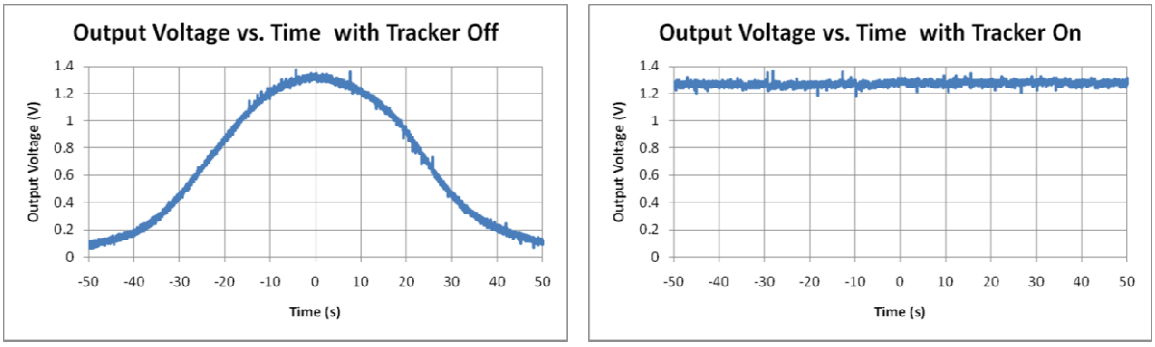

Figure V-2: Tracking linear motion of 1.5˚/s using hill-climbing algorithm.
No tracking (left), tracking (right).

In order to experimentally verify this algorithm I used the same setup as in the previous section, the PMSC mounted on rotation stage and illuminated a Xe arc lamp solar simulator. Seen above in Figure V-2 is the output voltage from the solar cell as a function of time when the rotation stage is rotating at 1.5˚/s with and without the use of the hill-climbing algorithm. In this case rotation was only with respect to one axis, but the algorithm is easily extended to two axes.

V.C Experimental Results using Solar Illumination

In order to track the sun, as opposed to a source moving with a constant speed in one axis, a few modifications and additions needed to be added to the hill-climbing algorithm. The addition of tracking in two-axes adds the complication that one of the axes of the system controls rotation and translation of one axis. This difficulty is overcome by occasionally correcting for rotational errors by moving one of the cams in the pair back 100 steps, then forward 50, to account for backlash, then scanning forward to find a peak.

The other notable modification is the rate at which the algorithm is run. As mentioned, this depends on how quickly the sun is moving with respect to each axis. Plotted in Figure V-3 below is the azimuth and altitude vs. time as well as the change in altitude and azimuth per

minute vs. time from 8AM to 4PM. From this data I chose to run the algorithm for the axis that is primarily azimuth to once every 10 seconds, and for the axis that is primarily altitude, every 25 seconds.

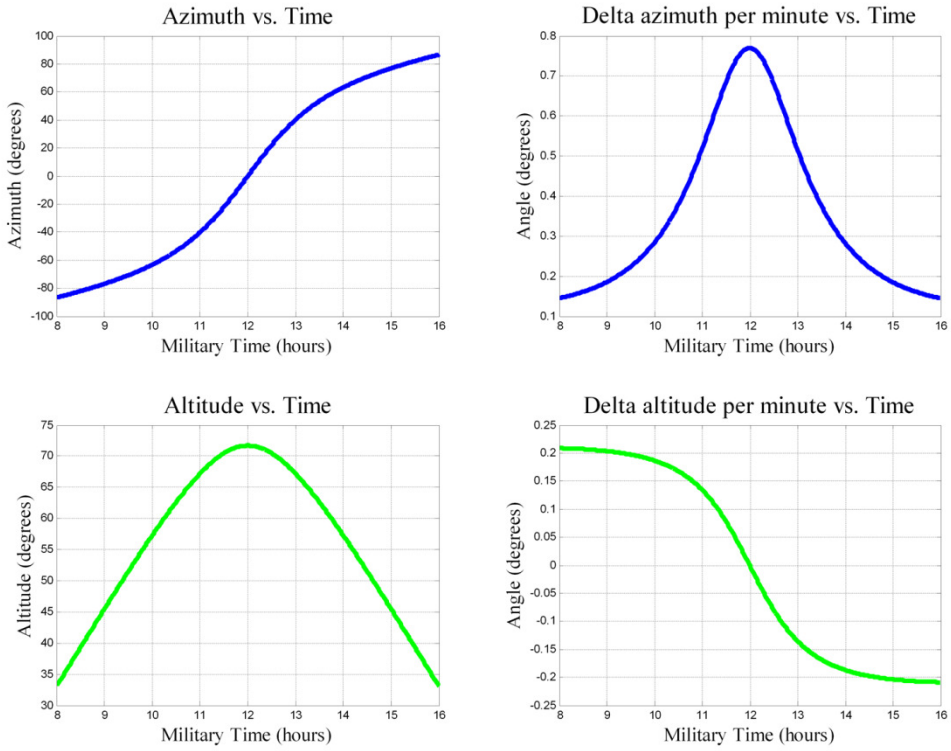

Figure V-3: Change in azimuth and altitude vs. time on May 15th, 2011 in San Diego, CA.

I tested my algorithm outside by mounting the PMSC micro-tracking platform on a tri-pod, aligning the tri-pod normal to the sun, manually aligning the PMSC using push-button input, and enabling the algorithm. The results plotted in Figure V-5 below were taken over the course of an hour starting at 1:45PM on May 25th, 2011. The measured output from the A/D converter was sent through a serial link back to the laptop over a UART to USB connection at 1Mbps. The output consisted of how many counts since the last transmission, how many steps taken in which axis if any, and power output. Also plotted on the figure below is the expected

output resulting from the loss due to the cosine of the angle off-normal multiplied by the reduction in intensity over time, multiplied by the off-axis efficiency of PMSC.

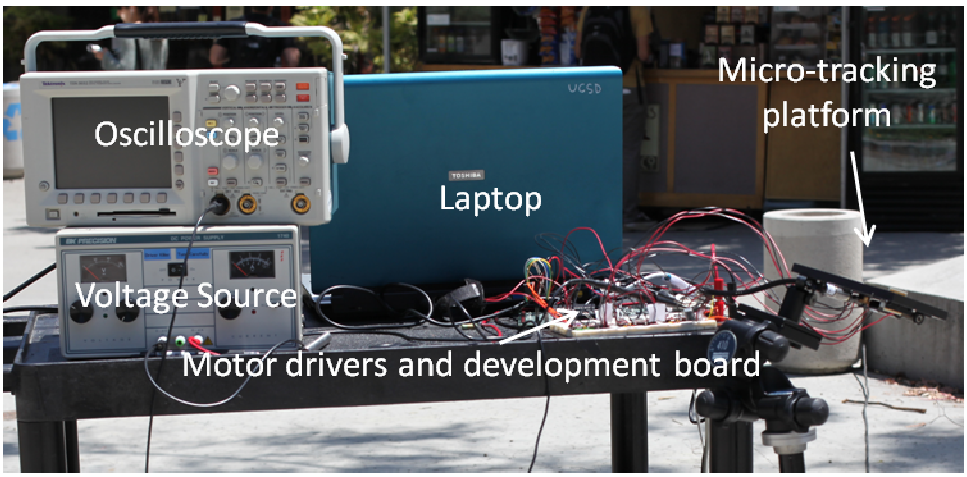

Figure V-4: Experimental setup for taking measurement on-sun.

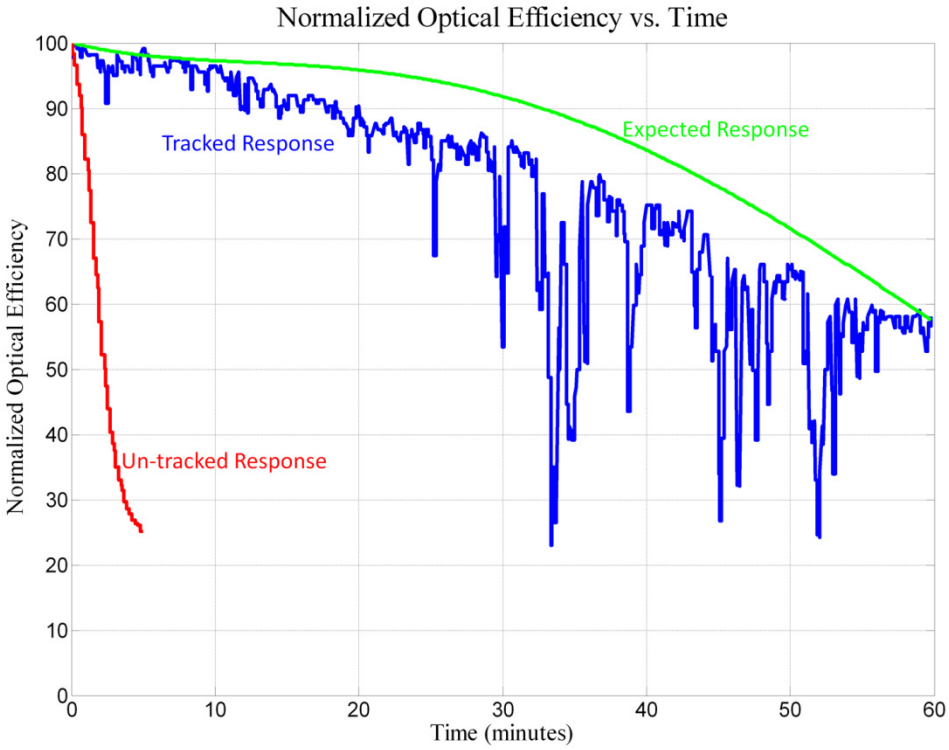

Figure V-5: Plot of normalized optical efficiency vs. time for an un-tracked system (red) a system that tracks the sun using a hill-climbing algorithm (blue) and the expected response from the tracked system based on geometrical losses, intensity reduction, and off-axis performance of the system (green).

This algorithm is protected from cloud cover since the system measures the slope and not the absolute value of the output for whether it should proceed further or not. As seen in the plot above there are sections of lower output when cloud cover was significant but when the cloud cover abated the intensity returned to the curve it was on previously.

Chapter VI :

Conclusion

This thesis presents an investigation of micro-tracking with a planar micro-optic solar concentrator. Micro-tracking of a planar micro-optic solar concentrator has potential for use in many different configurations of CPV including in a fixed mechanical frame, on a single-axis polar tracker to track the declination angle, or in conjunction with mechanical two-axis tracker to relax tolerances.

I presented a design study of different micro-lenses and the areas where they excel and fail. Of particular interest is the reflective micro-lens design whose performance could be easily tailored for use in with a single-axis polar tracker or in a fixed frame tracking the sun with only micro-tracking. With respect to the coupling features there is room for ingenuity; they could be tailored to couple a broader range of angles, increase concentration, or decrease propagation loss.

The micro-tracking platform that I designed and fabricated could be scaled for use in a commercial system. The specific manner of actuation is flexible since the largest required translation is one lens pitch. This gives the designer the flexibility to tailor the lens array for a specific mechanical topology.

The only addition required for this system to be fully functioning in the field is a fast initial alignment algorithm. Creating an algorithm to accomplish this without the addition of any

hardware is a daunting task. With the addition positional feedback it would become tractable and with additional hardware, such as a GPS and accelerometer or a low-resolution CMOS sensor, the algorithm would become trivial.

Appendix A:

Source Code

This section includes source code for the two-axis hill-climbing algorithm used ultimately to track the sun. This code compiles in AVR Studio 4.0 and runs on a ATmega324p microcontroller. The other algorithms used are similar in nature and use many of the same functions.

A.A Defines.h

```
#define F_CPU 16000000UL
#define UART_BAUD 1000000

#define m1port PORTB
#define m1dir 0
#define m1step 1

#define m2port PORTB
#define m2dir 2
#define m2step 3

#define m3port PORTB
#define m3dir 4
#define m3step 5

#define enableport PORTB
#define yenable 6
#define xenable 7
```

```
#define ipin PINA
#define switchmode 0b10000000
#define switchdir 0b01000000
#define switchdir2 0b00100000

#define buttona 0b00000010
#define negbuttona 0b00000100
#define buttonb 0b00001000
#define negbuttonb 0b00010000
#define buttonc 0b00100000
#define negbuttonc 0b01000000
#define stepdiv 2
```

A.B Interface.h and Interface.c

Interface.h:

```
void stepm1 (void);
void stepm2 (void);
void stepm3 (void);
long measure_output (void);
```

Interface.c:

```
#include "defines.h"
#include "Solar_tracker.h"
#include <avr/io.h>
#include <util/delay.h>

void stepm1 (void)
{
    //move state forward or back
    if (m1steps>0)
    {
        m1port |= (1<<m1dir);
        m1steps--;
        m1pos++;
    }
    else if (m1steps<0)
    {
        m1port &= ~(1<<m1dir);
        m1steps++;
        m1pos--;
    }

    m1port |= (1<<m1step);
```

```
    _delay_ms(1);
    m1port &= ~(1<<m1step);
}


void stepm2 (void)
{
    //move state forward or back
    if (m2steps>0)
    {
        m2port |= (1<<m2dir);
        m2steps--;
        m2pos++;
    }
    else if (m2steps<0)
    {
        m2port &= ~(1<<m2dir);
        m2steps++;
        m2pos--;
    }

    m2port |= (1<<m2step);
    _delay_ms(1);
    m2port &= ~(1<<m2step);
}

void stepm3 (void)
{
    //move state forward or back
    if (m3steps>0)
    {
        m3port |= (1<<m3dir);
        m3steps--;
        m3pos++;
    }
    else if (m3steps<0)
    {
        m3port &= ~(1<<m3dir);
        m3steps++;
        m3pos--;
    }

    m3port |= (1<<m3step);
    _delay_ms(1);
    m3port &= ~(1<<m3step);
}

long measure_output (void)
{
```

```
    unsigned char ch;
    //Use ADC on portA to measure output from solar cell with resistor
    ch=0;
    //Select ADC Channel ch must be 0-7
    ch=ch&0b00000111;

    ADMUX|=ch;

    //Start Single conversion
    ADCSRA|=(1<<ADSC);

    //Wait for conversion to complete
    while(!(ADCSRA & (1<<ADIF)));

    //Clear ADIF by writing one to it
    ADCSRA|=(1<<ADIF);

    return ADCH;
}
```

A.C Uart.h and Uart.c

Uart.h:

```
void uart_init(void);
void USART_Transmit( unsigned char data );
```

Uart.c:

```
//section of code controlling uart operation

#include "defines.h"
#include <stdint.h>
#include <stdio.h>
#include <avr/io.h>
#include "uart.h"
#include <avr/interrupt.h>

/*
 * Initialize the UART to UART_BAUD Bd, tx/rx, 8N1.
 */

void uart_init(void)
{
    UBRR0L = (F_CPU / (16UL * UART_BAUD)) - 1;
```

```
    //do 2Mbps
    /*UCSR0A = _BV(U2X0);
    UBRR0L = 0;*/


    UBRR1L = (F_CPU / (16UL * UART_BAUD)) - 1;

    //initialize channel 2 for transmission with 2Mbps
    /*UCSR1A = _BV(U2X1);
    UBRR1L = 0;*/

    UCSR1B = _BV(TXEN1); /* tx enable */
}

void USART_Transmit( unsigned char data )//sends data on channel 1
{
    UDR1 = data;
}
```

A.D Solar_tracker.h and Solar_tracker.c

Solar_tracker.h:

```
void optimize (void);
void optimize2 (void);
void optimize3 (void);
void report(void);
void average(void);
int main (void);

extern volatile int m1steps, m2steps, m3steps;
extern volatile int m1pos, m2pos, m3pos;
```

Solar_tracker.c:

```
#include "defines.h"
#include "interface.h"
#include "Solar_tracker.h"
#include <ctype.h>
#include <stdint.h>
#include <stdio.h>
#include <avr/pgmspace.h>
#include <avr/io.h>
#include <util/delay.h>
```

```
#include <avr/interrupt.h>
#include "uart.h"

//steps to be taken
volatile int m1steps=0, m2steps=0, m3steps=0;

//current position counter
volatile int m1pos=0, m2pos=0, m3pos=0;
volatile long clock1=0, clock2=0;
volatile signed char toggle=1, toggle2=1;

volatile unsigned char i=0, go1=0,go2=0, go3=0, mode=1, yen=0, xen=0, count=0, code=0,
tick=0;
volatile int k=-1, j=0;

//val1 is current measured array to be averaged
volatile unsigned char measure[5];
volatile unsigned int current=0, tmax1=0, tmax2=0, old, old2, clock3=0;
volatile int cloc[3], tloc[3], rloc[3], startloc[3]={0,0,0};
volatile int tsteps=1*stepdiv;

//Timer overflow interrupt
ISR(TIMER2_OVF_vect)
{
        clock1+=1;
        clock2+=1;
        clock3+=1;
        if (clock1>=36000)  //~3600 per second, so 10 seconds for 36000
        {
            clock1=0;
            go1=1;
            tick=tick+1;
            if (tick>=18) //~3 minutes do rotation
            {
                tick=0;
                go3=1;
            }
        }
        if (clock2>=54000)  //~3600 per second, so 15 seconds for 54000
        {
            clock2=0;
            go2=1;
        }
        if          ((mode==1)&(m1steps==0)&(m2steps==0)&(m3steps==0)&((ipin          &
switchdir)==0x00))//switch direction of x-axis
        {
            while((ipin & switchdir)==0x00) {}

            if (toggle==1)
```

```
                toggle=2;
            else
                toggle=1;
        }
        if          ((mode==1)&(m1steps==0)&(m2steps==0)&(m3steps==0)&((ipin          &
switchdir2)==0x00))//switch direction of x-axis
        {
            while((ipin & switchdir2)==0x00) {}

            if (toggle2==1)
                toggle2=2;
            else
                toggle2=1;
        }
        if ((m1steps==0)&(m2steps==0)&(m3steps==0)&((ipin & switchmode)==0x00))
        {
            while((ipin & switchmode)==0x00) {}
                mode=2;
        }

        if (mode==2)
        {
            if ((ipin & buttona)==0x00)
            {
                m1steps++;
                if (yen==0)//if y-axis disabled, enable
                {
                    enableport &= ~(1<<yenable);
                    _delay_ms(1);
                    yen=1;
                }
            }
            else if ((ipin & negbuttona)==0x00)
            {
                m1steps--;
                if (yen==0)//if y-axis disabled, enable
                {
                    enableport &= ~(1<<yenable);
                    _delay_ms(1);
                    yen=1;
                }
            }
            if (m1steps==0)//if no steps on y-axis, disable
            {
                enableport |= (1<<yenable);
                yen=0;
            }

            if ((ipin & buttonb)==0x00)
```

```
{
    m2steps++;
    m3steps++;
    if (xen==0)//if x-axis disabled, enable
    {
        enableport &= ~(1<<xenable);
        _delay_ms(1);
        xen=1;
    }
}
else if ((ipin & negbuttonb)==0x00)
{
    m2steps--;
    m3steps--;
    if (xen==0)//if x-axis disabled, enable
    {
        enableport &= ~(1<<xenable);
        _delay_ms(1);
        xen=1;
    }
}

if ((ipin & buttonc)==0x00)
{
    m2steps++;
    if (xen==0)
    {
        enableport &= ~(1<<xenable);//if x-axis disabled, enable
        _delay_ms(1);
        xen=1;
    }
}
else if ((ipin & negbuttonc)==0x00)
{
    m2steps--;
    if (xen==0)
    {
        enableport &= ~(1<<xenable);//if x-axis disabled, enable
        _delay_ms(1);
        xen=1;
    }
}
if ((m2steps==0)&(m3steps==0))//if no steps on x-axis, disable
{
    enableport |= (1<<xenable);
    xen=0;
}
if (((ipin & buttona)==0x00)&((ipin & negbuttona)==0x00))
{
```

```
                mode=1;
            }
        }

        //if no steps needed, measure 5 samples, average and optimize
        if ((m1steps==0)&(m2steps==0)&(m3steps==0)&(go1==1)&(mode==1))
        {
            measure[i]=measure_output();
            i++;
            if (i==5)
            {
                i=0;
                optimize();
            }
        }
        else if ((m1steps==0)&(m2steps==0)&(m3steps==0)&(go2==1)&((mode==1)|(mode==3)))
        {
            if (mode==1)
                mode=3;

            measure[i]=measure_output();
            i++;
            if (i==5)
            {
                i=0;
                optimize2();
            }
        }
        else if ((m1steps==0)&(m2steps==0)&(m3steps==0)&(go3==1)&((mode==1)|(mode==4)))
        {
            if (mode!=4)
                mode=4;

            measure[i]=measure_output();
            i++;
            if (i==5)
            {
                i=0;
                optimize3();
            }
        }
        else
        {
            if (m1steps!=0) //num steps to be taken greater than 0 for motor 1
            {
                stepm1();
            }
```

```
            if (m2steps!=0) //num steps to be taken greater than 0 for motor 2
            {
                stepm2();
            }
            if (m3steps!=0) //num steps to be taken greater than 0 for motor 3
            {
                stepm3();
            }
        }


        TCNT2=0xFA;  //Preset count register to make overflow trigger sooner

}
void report(void)
{
        while ((UCSR1A & (1 << UDRE1)) == 0) {};
        // Send motion code
        USART_Transmit(code);
        while ((UCSR1A & (1 << UDRE1)) == 0) {};

        // Send steps
        USART_Transmit(count);
        while ((UCSR1A & (1 << UDRE1)) == 0) {};

        // Send clock high char
        USART_Transmit(*(((unsigned char *)&clock3) + 1));
        while ((UCSR1A & (1 << UDRE1)) == 0) {};

        // Send clock low char
        USART_Transmit(*((unsigned char *)&clock3));
        while ((UCSR1A & (1 << UDRE1)) == 0) {};

        // Send current value high char
        USART_Transmit(*(((unsigned char *)&current) + 1));
        while ((UCSR1A & (1 << UDRE1)) == 0) {};

        // Send current value low char
        USART_Transmit(*((unsigned char *)&current));
        clock3=0;
        count=0;
}

void average(void)
{
        old2=old;//2 steps ago now equal to one step ago
        old=current;//1 step ago is equal to old current
        current=0;   //initialize current at 0
```

```
        //add in measured current value averaged over 5 samples
        for (j=0; j<5; j++)
            current=current+measure[j];
}

void optimize (void)
{
        //disable interrupts
        cli();

        //initialize current value
        cloc[0]=m1pos;
        cloc[1]=m2pos;
        cloc[2]=m3pos;

        average();

        k++;

        if (((old2>=old)&(old>current))|(k>60))//if value decreasing, stop moving
        {
            k=-1;
            enableport |= (1<<yenable);//disable y-axis
            _delay_ms(1);
            yen=0;
            tmax1=current;
            go1=0;
            old2=0;
            old=0;
            code=3;
            report();
        }

        if ((tmax1==0)&(go1==1)) //go if tmax is reset
        {
            m1steps-=tsteps;
            count+=tsteps;
            if (yen==0) //if y-axis disabled, enable
            {
                enableport &= ~(1<<yenable);
                _delay_ms(5);
                yen=1;
            }
        }
        else if ((current<tmax1)&~(toggle2==2))  //if current value is less than previous max,
start moving
            tmax1=0;
        else //if system is not moving forward, and does not need to be started, turn off
        {
```

```
            tmax1=current;
            enableport |= (1<<yenable);
            _delay_ms(1);
            yen=0;
            go1=0;
            k=-1;
            code=2;
            report();
        }

        sei();
}

void optimize2 (void)
{
        //disable interrupts
        cli();

        //initialize current value
        cloc[0]=m1pos;
        cloc[1]=m2pos;
        cloc[2]=m3pos;

        average();

        k++;

        if (((old2>=old)&(old>current))|(k>60))//if value decreasing, stop moving
        {
            k=-1;
            enableport |= (1<<xenable);//disable y-axis
            _delay_ms(1);
            xen=0;
            tmax2=current;
            go2=0;
            old2=0;
            old=0;
            mode=1;
            code=1;
            report();
        }

        if ((tmax2==0)&(go2==1)) //go if tmax is reset
        {
            m2steps-=tsteps;
            m3steps-=tsteps;
            count+=tsteps;
            if (xen==0) //if y-axis disabled, enable
            {
```

```
                enableport &= ~(1<<xenable);
                _delay_ms(5);
                xen=1;
            }
        }
        else if ((current<tmax2)&~(toggle==2))  //if current value is less than previous max, start
moving
            tmax2=0;
        else //if system is not moving forward, and does not need to be started, turn off
        {
            tmax2=current;
            enableport |= (1<<xenable);
            _delay_ms(1);
            xen=0;
            go2=0;
            k=-1;
            mode=1;
            code=0;
            report();
        }

        sei();
}

void optimize3 (void)
{
        //disable interrupts
        cli();

        //initialize current value
        cloc[0]=m1pos;
        cloc[1]=m2pos;
        cloc[2]=m3pos;

        average();

        k++;

        if (k==0)
        {
            m2steps+=100;
            if (xen==0) //if y-axis disabled, enable
            {
                enableport &= ~(1<<xenable);
                _delay_ms(5);
                xen=1;
            }
        }
        else if (k==1)
```

```
{
    m2steps-=70;
    if (xen==0) //if y-axis disabled, enable
    {
        enableport &= ~(1<<xenable);
        _delay_ms(5);
        xen=1;
    }
}
else if (k==2)
{
    m2steps-=tsteps;
    count+=tsteps;
    if (xen==0) //if y-axis disabled, enable
    {
        enableport &= ~(1<<xenable);
        _delay_ms(5);
        xen=1;
    }
}
else if (((old2>=old)&(old>current))|(k>80))//if value decreasing, stop moving
{
    k=-1;
    enableport |= (1<<xenable);//disable y-axis
    _delay_ms(1);
    xen=0;
    go3=0;
    old2=0;
    old=0;
    mode=1;
    if (k<=17)
    {
        code=4;
        count=30-count;
    }
    else
    {
        code=5;
        count=count-30;
    }
    report();
}
else
{
    m2steps-=tsteps;
    count+=tsteps;
    if (xen==0) //if y-axis disabled, enable
    {
        enableport &= ~(1<<xenable);
```

```
                _delay_ms(5);
                xen=1;
            }
        }
        sei();
}

int main (void)
{
        //Make port B and D outputs
        DDRB = 0xFF;
        DDRD = 0xFF;

        //Make port A input and have pullups 3 MSBs
        DDRA = 0x00;
        PORTA= 0xE0;

        //Set motors to disabled
        enableport |= (1<<yenable);
        enableport |= (1<<xenable);

        //Setup ADC with 2.56 ref voltage and left adjusted output
        ADMUX=(1<<REFS0)|(1<<REFS1)|(1<<ADLAR);
        ADCSRA=(1<<ADEN)|(1<<ADPS2)|(ADPS1)|(ADPS0);

        TCCR2B |= (1 << CS20);  //Don't divide, so runs at 32Hz
        ASSR |= (1 << AS2);    //Use asynchronous clock source on tosc pin
        TIMSK2 |= (1 << TOIE2);  //Enable overflow interrupt
        TCNT2=0;    //Intialize Timer

        uart_init();

        //Enable Interrupts
        sei();

        while (1)
        {
        }
        return 1;
}
```

Appendix B:

ZEMAX Lens Prescription Data

B.A Prototype Singlet

GENERAL LENS DATA:
Surfaces : 4
Stop : 1
System Aperture : Entrance Pupil Diameter = 1
Glass Catalogs : SCHOTT MISC
Ray Aiming : Paraxial Reference, Cache On
X Pupil shift : 0
Y Pupil shift : 0
Z Pupil shift : 0
X Pupil compress : 0
Y Pupil compress : 0
Apodization : Uniform, factor = 0.00000E+000
Temperature (C) : 2.00000E+001
Pressure (ATM) : 1.00000E+000
Adjust Index Data To Environment : Off
Effective Focal Length : 2.980493 (in air at system temperature and pressure)
Effective Focal Length : 2.980493 (in image space)
Back Focal Length : 0.09807052
Total Track : 4.32
Image Space F/# : 2.980493
Paraxial Working F/# : 2.980493
Working F/# : 2.864181
Image Space NA : 0.1654456
Object Space NA : 5e-011
Stop Radius : 0.5
Paraxial Image Height : 2.50093
Paraxial Magnification : 0
Entrance Pupil Diameter : 1
Entrance Pupil Position : 0

Exit Pupil Diameter : 1
Exit Pupil Position : -2.882422
Field Type : Angle in degrees
Maximum Radial Field : 40
Primary Wavelength : 0.503 µm
Lens Units : Millimeters
Angular Magnification : 1

SURFACE DATA SUMMARY:

Surf	Type	Radius	Thickness	Glass	Diameter	Conic	Comment
OBJ	STANDARD	Infinity	Infinity		0	0	
STO	STANDARD	1.48	3.3	1.491668, 55.310192	1	0	
2	STANDARD	Infinity	0.02		3.219326	0	
3	STANDARD	Infinity	1	BK7	3.274848	0	
IMA	STANDARD	Infinity			4.560331	0	

SURFACE DATA DETAIL:
Surface OBJ STANDARD
Surface STO STANDARD
Aperture : User Aperture
Aperture File : HEXAGON_UNIT1.UDA
Aperture Scale : 0.5
User Aper Data : 0.25 -0.4330127
User Aper Data : -0.25 -0.4330127
User Aper Data : -0.5 3.8285889e-016
User Aper Data : -0.25 0.4330127
User Aper Data : 0.25 0.4330127
User Aper Data : 0.5 -1.209807e-015
User Aper Data : 0 0
Surface 2 STANDARD
Surface 3 STANDARD
Surface IMA STANDARD

B.B Optimized Singlet

GENERAL LENS DATA:
Surfaces : 4
Stop : 1
System Aperture : Entrance Pupil Diameter = 1
Glass Catalogs : SCHOTT MISC
Ray Aiming : Paraxial Reference, Cache On
X Pupil shift : 0
Y Pupil shift : 0
Z Pupil shift : 0
X Pupil compress : 0
Y Pupil compress : 0

Apodization : Uniform, factor = 0.00000E+000
Temperature (C) : 2.00000E+001
Pressure (ATM) : 1.00000E+000
Adjust Index Data To Environment : Off
Effective Focal Length : 2.831193 (in air at system temperature and pressure)
Effective Focal Length : 4.59842 (in image space)
Back Focal Length : 0.304126
Total Track : 4.020031
Image Space F/# : 2.831193
Paraxial Working F/# : 2.831193
Working F/# : 2.95073
Image Space NA : 0.1755692
Object Space NA : 5e-011
Stop Radius : 0.5
Paraxial Image Height : 2.375653
Paraxial Magnification : 0
Entrance Pupil Diameter : 1
Entrance Pupil Position : 0
Exit Pupil Diameter : 1
Exit Pupil Position : -4.294294
Field Type : Angle in degrees
Maximum Radial Field : 40
Primary Wavelength : 0.545 µm
Lens Units : Millimeters
Angular Magnification : 0.6156883

SURFACE DATA SUMMARY:

Surf	Type	Radius	Thickness	Glass	Diameter	Conic	Comment
OBJ	STANDARD	Infinity	Infinity		0	0	
STO	EVENASPH	4.685568	3.000031	1.491668, 55.310192	1	67.30525	
2	STANDARD	Infinity	0.02		2.845534	0	
3	STANDARD	Infinity	1	F2	2.885565	0	
IMA	STANDARD	Infinity		F2	4.02307	0	

SURFACE DATA DETAIL:
Surface OBJ STANDARD
Aperture : User Aperture
Aperture File : HEXAGON_UNIT1.UDA
Aperture Scale : 0.5
User Aper Data : 0.25 -0.4330127
User Aper Data : -0.25 -0.4330127
User Aper Data : -0.5 3.8285889e-016
User Aper Data : -0.25 0.4330127
User Aper Data : 0.25 0.4330127
User Aper Data : 0.5 -1.209807e-015
User Aper Data : 0 0
Surface STO EVENASPH
Coeff on r 2 : 0.25089781
Coeff on r 4 : -0.097701855

Coeff on r 6 :   -0.31442551
Coeff on r 8 :   0.71449507
Coeff on r 10 :   5.1471249
Coeff on r 12 :   9.0200355
Coeff on r 14 :   -29.204151
Coeff on r 16 :   -343.34046
Aperture   : User Aperture
Aperture File : HEXAGON_UNIT1.UDA
Aperture Scale :   0.5
User Aper Data :   0.25   -0.4330127
User Aper Data :   -0.25   -0.4330127
User Aper Data :   -0.5   3.8285889e-016
User Aper Data :   -0.25   0.4330127
User Aper Data :   0.25   0.4330127
User Aper Data :   0.5   -1.209807e-015
User Aper Data :   0   0
Surface   2 STANDARD
Aperture   : Circular Aperture
Minimum Radius :   0
Maximum Radius :   2
Surface   3 STANDARD
Aperture   : Circular Aperture
Minimum Radius :   0
Maximum Radius :   2
Surface IMA STANDARD
Aperture   : Circular Aperture
Minimum Radius :   0
Maximum Radius :   2

B.C Refractive Doublet

GENERAL LENS DATA:

Surfaces   :   6
Stop   :   1
System Aperture   : Entrance Pupil Diameter = 1
Glass Catalogs   : SCHOTT MISC
Ray Aiming   : Paraxial Reference, Cache On
X Pupil shift   :   0
Y Pupil shift   :   0
Z Pupil shift   :   0
X Pupil compress   :   0
Y Pupil compress   :   0
Apodization   : Uniform, factor =   0.00000E+000
Temperature (C)   :   2.00000E+001
Pressure (ATM)   :   1.00000E+000

Adjust Index Data To Environment : Off
Effective Focal Length : 6.769483e-019 (in air at system temperature and pressure)
Effective Focal Length : 1.028134e-018 (in image space)
Back Focal Length : 7.123205e-019
Total Track : 1.721068
Image Space F/# : 6.769483e-019
Paraxial Working F/# : 6.769483e-019
Working F/# : 1.141159
Image Space NA : 1.518777
Object Space NA : 5e-011
Stop Radius : 0.5
Paraxial Image Height : 0.2578665
Paraxial Magnification : 0
Entrance Pupil Diameter : 1
Entrance Pupil Position : 0
Exit Pupil Diameter : 0.6913578
Exit Pupil Position : -1.107792
Field Type : Angle in degrees
Maximum Radial Field : 30
Primary Wavelength : 0.545 µm
Lens Units : Millimeters
Angular Magnification : -6.270182e+017

SURFACE DATA SUMMARY:

Surf	Type	Radius	Thickness	Glass	Diameter	Conic	Comment
OBJ	STANDARD	Infinity	Infinity		0	0	
STO	EVENASPH	0.6885751	0.5063681	1.491668, 55.310192	1	0.3461748	lens 1
2	EVENASPH	Infinity	0.1076688		1	0	
3	EVENASPH	2.766508e-019	0.09703082	1.584700, 27.560000	1	-1958.409	lens 2
4	STANDARD	Infinity	0.01		1	0	clad
5	STANDARD	Infinity	1	BK7	2	0	waveguide
IMA	STANDARD	Infinity		BK7	1.557652	0	

SURFACE DATA DETAIL:

Surface OBJ STANDARD
Surface STO EVENASPH lens 1
Coating : I.95
Coeff on r 2 : -0.029827688
Coeff on r 4 : -0.078499786
Coeff on r 6 : 0.08276271
Coeff on r 8 : -0.81044852
Coeff on r 10 : -2.4078362
Coeff on r 12 : -3.6424644
Coeff on r 14 : -3.8673842
Coeff on r 16 : 1.1619632
Aperture : User Aperture

Aperture File : HEXAGON_UNIT1.UDA
Aperture Scale : 0.5
User Aper Data : 0.25 -0.4330127
User Aper Data : -0.25 -0.4330127
User Aper Data : -0.5 3.8285889e-016
User Aper Data : -0.25 0.4330127
User Aper Data : 0.25 0.4330127
User Aper Data : 0.5 -1.209807e-015
User Aper Data : 0 0
Surface 2 EVENASPH
Coeff on r 2 : 0
Coeff on r 4 : 0
Coeff on r 6 : 0
Coeff on r 8 : 0
Coeff on r 10 : 0
Coeff on r 12 : 0
Coeff on r 14 : 0
Coeff on r 16 : 0
Aperture : Floating Aperture
Maximum Radius : 0.5
Surface 3 EVENASPH lens 2
Coating : I.95
Coeff on r 2 : 0.00083444623
Coeff on r 4 : 0.19751216
Coeff on r 6 : -1.8429257
Coeff on r 8 : -12.250615
Coeff on r 10 : -26.694302
Coeff on r 12 : -73.651094
Coeff on r 14 : -76.913622
Coeff on r 16 : 64.85833
Aperture : User Aperture, Pickup From Surface 1
Aperture File : HEXAGON_UNIT1.UDA
Aperture Scale : 0.5
User Aper Data : 0.25 -0.4330127
User Aper Data : -0.25 -0.4330127
User Aper Data : -0.5 3.8285889e-016
User Aper Data : -0.25 0.4330127
User Aper Data : 0.25 0.4330127
User Aper Data : 0.5 -1.209807e-015
User Aper Data : 0 0
Surface 4 STANDARD clad
Aperture : Floating Aperture
Maximum Radius : 0.5
Surface 5 STANDARD waveguide
Aperture : Floating Aperture
Maximum Radius : 1
Surface IMA STANDARD

B.D Reflective 24°

GENERAL LENS DATA:

Surfaces : 8
Stop : 5
System Aperture : Entrance Pupil Diameter = 1
Glass Catalogs : SCHOTT MISC
Ray Aiming : Paraxial Reference, Cache On
X Pupil shift : 0
Y Pupil shift : 0
Z Pupil shift : 0
X Pupil compress : 0
Y Pupil compress : 0
Apodization : Uniform, factor = 0.00000E+000
Temperature (C) : 2.00000E+001
Pressure (ATM) : 1.00000E+000
Adjust Index Data To Environment : Off
Effective Focal Length : 2.213847 (in air at system temperature and pressure)
Effective Focal Length : 3.36234 (in image space)
Back Focal Length : -0.1352498
Total Track : 3.685595
Image Space F/# : 2.213847
Paraxial Working F/# : 2.213847
Working F/# : 2.231017
Image Space NA : 0.2233947
Object Space NA : 5e-011
Stop Radius : 0.5
Paraxial Image Height : 1.857638
Paraxial Magnification : 0
Entrance Pupil Diameter : 1
Entrance Pupil Position : 2.624795
Exit Pupil Diameter : 1
Exit Pupil Position : 3.22709
Field Type : Angle in degrees
Maximum Radial Field : 40
Primary Wavelength : 0.545 µm
Lens Units : Millimeters
Angular Magnification : -0.6584244

SURFACE DATA SUMMARY:

Surf	Type	Radius	Thickness	Glass	Diameter	Conic	Comment
OBJ	STANDARD	Infinity	Infinity		0	0	
1	STANDARD	Infinity	0.5		4.882138	0	
2	STANDARD	Infinity	1	BK7	4.043038	0	waveguide
3	STANDARD	Infinity	0.01		3.097294	0	

4 STANDARD	Infinity	2.175595	1.491668, 55.310192		3.080512	0
STO EVENASPH	-7.111812	-2.175595		MIRROR	1	9.370862
6 STANDARD	Infinity	-0.01			3.097294	0
7 STANDARD	Infinity	-1		BK7	2.338414	0
IMA STANDARD	Infinity			BK7	3.317933	0

SURFACE DATA DETAIL:

Surface OBJ STANDARD
Surface 1 STANDARD
Surface 2 STANDARD waveguide
Surface 3 STANDARD
Surface 4 STANDARD
Surface STO EVENASPH
Coeff on r 2 : -0.0052882412
Coeff on r 4 : 0.0036741606
Coeff on r 6 : -0.0020591814
Coeff on r 8 : 0.088723379
Coeff on r 10 : -0.77521294
Coeff on r 12 : 3.0054595
Coeff on r 14 : -5.132395
Coeff on r 16 : 2.7341426
Aperture : User Aperture
Aperture File : HEXAGON_UNIT1.UDA
Aperture Scale : 0.5
User Aper Data : 0.25 -0.4330127
User Aper Data : -0.25 -0.4330127
User Aper Data : -0.5 3.8285889e-016
User Aper Data : -0.25 0.4330127
User Aper Data : 0.25 0.4330127
User Aper Data : 0.5 -1.209807e-015
User Aper Data : 0 0
Surface 6 STANDARD
Surface 7 STANDARD
Surface IMA STANDARD

B.E Reflective 40°

GENERAL LENS DATA:

Surfaces : 7
Stop : 4
System Aperture : Entrance Pupil Diameter = 1
Glass Catalogs : SCHOTT MISC
Ray Aiming : Paraxial Reference, Cache On
X Pupil shift : 0

Y Pupil shift : 0
Z Pupil shift : 0
X Pupil compress : 0
Y Pupil compress : 0
Apodization : Uniform, factor = 0.00000E+000
Temperature (C) : 2.00000E+001
Pressure (ATM) : 1.00000E+000
Adjust Index Data To Environment : Off
Effective Focal Length : 2.427974 (in air at system temperature and pressure)
Effective Focal Length : 3.687551 (in image space)
Back Focal Length : -0.4717705
Total Track : 3.174471
Image Space F/# : 2.427974
Paraxial Working F/# : 2.427974
Working F/# : 2.384946
Image Space NA : 0.2040657
Object Space NA : 5e-011
Stop Radius : 0.5
Paraxial Image Height : 2.037312
Paraxial Magnification : 0
Entrance Pupil Diameter : 1
Entrance Pupil Position : 2.117348
Exit Pupil Diameter : 1
Exit Pupil Position : 3.215781
Field Type : Angle in degrees
Maximum Radial Field : 40
Primary Wavelength : 0.545 µm
Lens Units : Millimeters
Angular Magnification : -0.6584244

SURFACE DATA SUMMARY:

Surf	Type	Radius	Thickness	Glass	Diameter	Conic	Comment
OBJ	STANDARD	Infinity	Infinity		0	0	
1	STANDARD	Infinity	1	BK7	4.033651	0	waveguide
2	STANDARD	Infinity	0.01		3.087906	0	
3	STANDARD	Infinity	2.164471	1.491668, 55.310192	3.071124	0	
STO	EVENASPH	-7.304022	-2.164471	MIRROR	1	27.65132	
5	STANDARD	Infinity	-0.01		3.087906	0	
6	STANDARD	Infinity	-1	BK7	2.378953	0	
IMA	STANDARD	Infinity		BK7	3.214471	0	

SURFACE DATA DETAIL:

Surface OBJ STANDARD
Surface 1 STANDARD waveguide
Surface 2 STANDARD
Surface 3 STANDARD

Surface STO EVENASPH
Coeff on r 2 :   -0.00047164076
Coeff on r 4 :   0.00083152874
Coeff on r 6 :   -0.0011622644
Coeff on r 8 :   0.042765865
Coeff on r 10 :   0.21103886
Coeff on r 12 :   0.72567722
Coeff on r 14 :   2.3026553
Coeff on r 16 :   -23.869934
Aperture   : User Aperture
Aperture File : HEXAGON_UNIT1.UDA
Aperture Scale :   0.5
User Aper Data :   0.25   -0.4330127
User Aper Data :   -0.25   -0.4330127
User Aper Data :   -0.5   3.8285889e-016
User Aper Data :   -0.25   0.4330127
User Aper Data :   0.25   0.4330127
User Aper Data :   0.5   -1.209807e-015
User Aper Data :   0   0
Surface   5 STANDARD
Surface   6 STANDARD
Surface IMA STANDARD

Bibliography

[1] J. H. Karp, E. J. Tremblay, and J. E. Ford, "Planar micro-optic solar concentrator," Optics Express, Vol. 18, Issue 2, 1122-1133 (2010)

[2] R. Winston, J. C. Minano, W. T. Welford, P. Benitez, *Nonimaging Optics* (Academic Press, 2004).

[3] A.W. Bett, and H. Lerchenmuller, "The FLATCON System from Concentrix Solar," in *Concentrator Photovoltaics*, A.L. Luque, and V.M. Andreev, (Springer, Berlin, 2007).

[4] Concentrix Solar CX-P6 Data Sheet (2010).

[5] J. H. Karp, E. J. Tremblay, and J. E. Ford, "Micro-Optic Solar Concentration and Next-Generation Prototypes," IEEE Photovoltaic Specialists Conference (2010).

[6] http://www.morgansolar.com

[7] http://www.banyanenergy.com

[8] B. L. Unger, G. R. Schmidt, and D. T. Moore, "Dimpled Planar Lightguide Solar Concentrators," in International Optical Design Conference, OSA Technical Digest (CD) (Optical Society of America, 2010), paper ITuE5P.

[9] J. H. Karp, E. J. Tremblay, J. M. Hallas, and J. E. Ford, "Orthogonal and secondary concentration in planar micro-optic solar collectors," Opt. Express 19, A673-A685 (2011)

[10] J. M. Hallas, J. H. Karp, E. J. Tremblay and J. E. Ford, "Lateral translation micro-tracking of planar micro-optic solar concentrator", Proc. SPIE 7769, 776904 (2010)

[11] K. A. Baker, J. H. Karp, E. J. Tremblay, J. M. Hallas, and J. E. Ford, “Reactive self-tracking solar concentration: design and materials characterization,” Energy Express (in preparation).

[12] J. M. Hallas, J. H. Karp, K. A. Baker, E. J. Tremblay, and J. E. Ford, “Micro-tracking of planar micro-optic solar concentrator,” Optics Express (in preparation).

[13] F. Duerr, Y. Meuret, and H. Thienpont, "Tracking integration in concentrating photovoltaics using laterally moving optics," Opt. Express 19, A207-A218 (2011)

[14] V. C. Coffey “Solar Concentrators: Using optics to boost photovoltaics,” Optics and Photonics News, Vol. 22, Issue 1, pp. 22-27 (2011).

[15] ADM1220 Motor Datasheet: http://www.micromo.com/datasheets/Stepper%20Motors/ADM_1220_PCS.pdf